


## Dissipative Dirac matrix spin model in two dimensions

Jyotsna Gidugu<sup>\*</sup> and Daniel P. Arovas<sup>†</sup>

*Department of Physics, University of California San Diego, La Jolla, California 92093, USA*

 (Received 13 September 2023; accepted 9 January 2024; published 9 February 2024)

We generalize the recent work of Shibata and Katsura [Phys. Rev. B **99**, 174303 (2019)], who considered a  $S = \frac{1}{2}$  chain with alternating  $XX$  and  $YY$  couplings in the presence of dephasing, the dynamics of which are described by the GKLS master equation. Their model is equivalent to a non-Hermitian system described by the Kitaev formulation [Kitaev, Ann. Phys. **321**, 2 (2006)] in terms of a single Majorana species hopping on a two-leg ladder in the presence of a nondynamical  $\mathbb{Z}_2$  gauge field. Our generalization involves Dirac gamma matrix “spin” operators on the square lattice and maps onto a non-Hermitian square lattice bilayer which is also Kitaev solvable. We describe the exponentially many nonequilibrium steady states in this model. We identify how the spin degrees of freedom can be accounted for in the two-dimensional model in terms of the gauge-invariant quantities and then proceed to study the Liouvillian spectrum. We use simulated annealing to estimate the Liouvillian gap and the first decay modes for large system sizes. We observe a transition in the first decay modes, similar to that in the work of Shibata and Katsura. The results we obtain are compared to the results we obtained from a perturbative analysis for small and large values of the dissipation strength.

DOI: [10.1103/PhysRevA.109.022212](https://doi.org/10.1103/PhysRevA.109.022212)

### I. INTRODUCTION

Open quantum systems afford us the opportunity to study phenomena such as relaxational quantum dynamics for systems coupled to a bath [1]. Typically this involves “integrating out” or eliminating in some way the bath degrees of freedom, resulting in a dynamics for the system itself in terms of its reduced density matrix:  $\dot{\rho} = \mathcal{L}\rho$ , where  $\mathcal{L}$  is the Liouvillian operator. At long times, the system relaxes to a nonequilibrium steady state (NESS); the existence of a NESS is guaranteed by the dynamics, but under special circumstances owing to, for example, extra conserved quantities, the NESS may not be unique.

For noninteracting systems, hybridization with the bath degrees of freedom still results in a solvable (quadratic) model [2]. For interacting systems, solvable models are rare, and numerical approaches are challenging. This is especially true for density matrix evolution since one must keep track of not just populations  $|\alpha\rangle\langle\alpha|$  but also the coherences  $|\alpha\rangle\langle\beta|$  with  $\alpha \neq \beta$ , effectively squaring the size of the problem vis-à-vis the system’s Hilbert space dimension.

Recently, Shibata and Katsura (SK) [3] described a model of open system dynamics based on the GKLS master equation [4] which, though interacting, is solvable in the sense of Kitaev’s celebrated honeycomb lattice Hamiltonian model [5]. That is, the evolution of  $\rho(t)$  under the Liouvillian  $\mathcal{L}$  is effectively described by a noninteracting dynamics in the presence of a static  $\mathbb{Z}_2$  gauge field. Although in each gauge sector the evolution is described by a quadratic, albeit non-Hermitian, Hamiltonian, there are exponentially many gauge

sectors to evaluate (which in general have no discrete space group symmetries), and in this sense the general problem is intractable. For the Hermitian Kitaev model, often the ground state may be ascertained with help from a remarkable theorem by Lieb [6], which provides valuable information regarding much of the gauge-invariant content of the ground state, i.e., the  $\mathbb{Z}_2$  plaquette fluxes. For the non-Hermitian case, however, we know of no generalization of Lieb’s theorem which constrains the gauge-invariant content of, say, the longest-lived decaying density matrix. Thus, in general one must resort to numerics if one is interested in the complex spectrum of  $\mathcal{L}$ .

The Shibata-Katsura construction involves a  $S = \frac{1}{2}$  chain where each site is coupled to an environmental bath. Within the GKLS formalism, this results in an effective two leg ladder system, where one leg corresponds to the bra states and the other to the ket states of the density matrix, and the rungs of the ladder contribute non-Hermitian terms which result from the effective elimination of the bath degrees of freedom. The ladder is thus threefold coordinated, and the model is constructed so that it satisfies the Kitaev solvability criteria (Sec. IIC). Our main goal is to introduce and analyze a generalization of the SK model to two space dimensions, based on a  $4 \times 4$  gamma matrix generalization of the Hamiltonian Kitaev model [7,8]. As the dissipative SK model is described by non-Hermitian Hamiltonian evolution on the ladder, our model is described by such an evolution on a square lattice bilayer. As we shall see, while our model is a direct analog of the SK model, it also entails some important differences—in particular, an extensive number of conserved quantities leading to exponentially many NESS [9].

We first discuss various preliminaries, including the GKLS master equation, its vectorization and description in terms of non-Hermitian Hamiltonian evolution on a product Hilbert space, the Shibata-Katsura model, gamma matrix

<sup>\*</sup>gidugu@ucsd.edu

<sup>†</sup>darovas@ucsd.edu

generalizations of the Kitaev honeycomb model, and finally our extension of the SK model to a dissipative square lattice model involving  $4 \times 4$  Dirac matrix “spin” operators.

Recently, two analyses of a largely equivalent model appeared [10,11]. These papers and our work discuss models with different Hamiltonians and Lindblad operators, although there are some features common to all three, such as the behavior of the Liouvillian gap at small and large dissipation, various conserved quantities, steady states and some approaches toward understanding other modes of the system. Our model is solvable in the Kitaev sense in that it is equivalent to a noninteracting non-Hermitian Majorana system in the presence of a background  $\mathbb{Z}_2$  gauge field. While the Hamiltonian may be diagonalized within each gauge sector, there are exponentially many such sectors. We perform a limited search of the gauge sectors using Monte Carlo methods in an effort to obtain the smallest relaxation rate to the (highly degenerate) block of nonequilibrium steady states, i.e., the Liouvillian gap. Due to the local constraints imposed by the parton representation of the spin operators in terms of Majorana fermions, some solutions are unphysical in that they violate these constraints. As noted in Ref. [11], it is as yet unknown how to assess which solutions are physical from the gauge-invariant data alone. In the limits of small and large dissipation, we derive analytical results which can be compared with the numerics. In addition to the exponentially many gauge sectors, there are also exponentially many NESS, and we identify all of them in terms of conserved quantities.

## II. PRELIMINARIES

### A. The GKLS master equation

An open quantum system  $\mathbf{S}$  is one which unitarily evolves with an environment  $\mathbf{E}$  under a Hamiltonian  $H = H_{\mathbf{S}} + H_{\mathbf{E}} + H_{\text{int}}$ , where  $H_{\text{int}}$  couples  $\mathbf{S}$  and  $\mathbf{E}$ . The expectation of any operator  $\mathcal{O}$  restricted to  $\mathbf{S}$  is given by  $\langle \mathcal{O}(t) \rangle = \text{Tr}(\varrho_{\mathbf{S}}(t) \mathcal{O})$ , where  $\varrho_{\mathbf{S}}(t)$  is the time-dependent reduced density matrix of  $\mathbf{S}$ , i.e.,  $\varrho_{\mathbf{S}}(t) = \text{Tr}_{\mathbf{E}} \varrho_{\mathbf{U}}(t)$ , where  $\varrho_{\mathbf{U}}(t)$  is the full density matrix describing the “universe”  $\mathbf{U} = \mathbf{S} \cup \mathbf{E}$ . Under certain assumptions, the dynamics of the system’s reduced density matrix is described by the GKLS master equation [1,4],

$$\frac{d\varrho}{dt} = -i[H, \varrho] + \sum_a \left( L_a \varrho L_a^\dagger - \frac{1}{2} L_a^\dagger L_a \varrho - \frac{1}{2} \varrho L_a^\dagger L_a \right). \quad (1)$$

Here and henceforth we drop the subscript  $\mathbf{S}$  on  $\varrho_{\mathbf{S}}$ . The  $\{L_a\}$  are the Lindblad jump operators, which describe the effects of the system-environment coupling on  $\varrho$  after the environment is traced out.  $H$  is the “Lamb shift Hamiltonian,” which commutes with  $H_{\mathbf{S}}$  and includes renormalizations of the system’s unperturbed energy levels resulting from the environmental couplings. In the absence of all such couplings, we recover the usual Liouville evolution  $\dot{\varrho} = -i[H_{\mathbf{S}}, \varrho]$ .

The full GKLS evolution in Eq. (1) is of the form  $\dot{\varrho} = \mathcal{L}\varrho$ . Assuming  $\mathcal{L}$  is time-independent, one may formally write  $\varrho(t) = \exp(\mathcal{L}t)\varrho(0)$ , which defines for each  $t$  a map  $\Phi_t : \varrho(0) \mapsto \varrho(t)$  which possesses the following salient properties: (i) linearity, (ii) trace-preserving, (iii) Hermiticity preserving, and (iv) complete positivity [1]. Writing  $\varrho(t) = \sum_{j,k} \varrho_{jk}(t) |j\rangle\langle k|$  in terms of basis states, we may write  $\dot{\varrho}_{jk} =$

$\mathcal{L}_{jk,lm} \varrho_{lm}$ , where  $\mathcal{L}_{jk,lm}$  is a supermatrix of dimension  $N^2$ , where  $N$  is the dimension of the single, i.e., not doubled basis, and  $(jk)/(lm)$  are composite indices. Generically  $\mathcal{L}$  is not a normal matrix, i.e.,  $[\mathcal{L}, \mathcal{L}^\dagger] \neq 0$ , and its eigenvalues  $\Lambda_a$  may be complex. However, since the evolution is trace preserving, one has that  $\delta_{jk}$  is a left eigenvector of  $\mathcal{L}$  with eigenvalue zero. The corresponding right eigenvector is the NESS,  $\varrho_{lm}^{\text{NESS}}$ . Under special circumstances there may be more than one NESS [12]. Positivity entails that  $\text{Re} \Lambda_a \leq 0$  for each eigenvalue of the Liouvillian  $\mathcal{L}$ .

When each jump operator is normal (i.e., it commutes with its Hermitian conjugate), then from Eq. (1) we have that the infinite temperature state  $\varrho \propto \mathbb{1}$  is a valid NESS. Furthermore, if  $H$  as well as all the jump operators commute with a set of independent projectors  $\{P_s\}$  with  $s \in \{1, \dots, K\}$ , then any density matrix of the form

$$\varrho = c_0 \mathbb{1} + \sum_{s=1}^K c_s P_s \quad (2)$$

is also a valid NESS (subject to normalization). This shall be the case for the model we investigate below. Thus we shall describe a system where there is relaxation to a degenerate block of NESS. While such solutions to GKLS depend on the form of  $H$  and the jump operators  $\{L_a\}$ , they are independent of the various coupling constants (so long as they remain finite), and we shall consider them all to be infinite temperature states.

### B. Equivalent non-Hermitian Hamiltonian

Any density matrix  $\varrho = \sum_{m,n} \varrho_{mn} |m\rangle\langle n|$  may be represented in vector form as

$$\varrho \longrightarrow |\varrho\rangle \equiv \sum_{m,n} \varrho_{mn} |m\rangle \otimes |n\rangle. \quad (3)$$

Thus, the bra vector  $\langle n|$  is replaced by the corresponding ket vector  $|n\rangle$ , i.e.,  $|m\rangle\langle n| \rightarrow |m\rangle \otimes |n\rangle$ . If  $B$  is any operator, then under vectorization, then we have

$$\begin{aligned} \langle n|B &= \sum_k \langle n|B|k\rangle \langle k| \\ &\longrightarrow \sum_k |k\rangle \langle k|B^\dagger |n\rangle = B^\dagger |n\rangle. \end{aligned} \quad (4)$$

The GKLS master equation [Eq. (1)] then takes the vectorized form

$$i \frac{d}{dt} |\varrho\rangle = \mathcal{W} |\varrho\rangle, \quad (5)$$

where [13]

$$\begin{aligned} \mathcal{W} &= H \otimes \mathbb{1} - \mathbb{1} \otimes H^\dagger \\ &+ i \sum_r \left( L_r \otimes L_r^* - \frac{1}{2} L_r^\dagger L_r \otimes \mathbb{1} - \mathbb{1} \otimes \frac{1}{2} L_r^\dagger L_r^* \right). \end{aligned} \quad (6)$$

Note that operators  $\mathcal{O}$  acting on the  $|n\rangle$  component of the product  $|m\rangle \otimes |n\rangle$  appear as transposes  $\mathcal{O}^\dagger$ , since they would

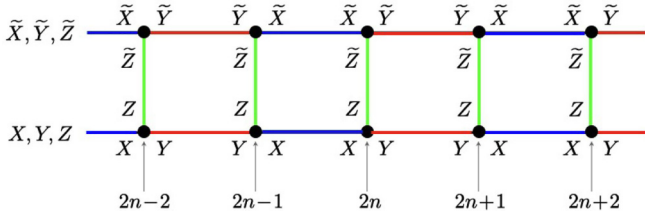


FIG. 1. The Shibata-Katsura ladder (see text for description).

normally act to the left on  $\langle n |$ . Equation (5) takes the form of an effective Schrödinger equation, with  $|\varrho(t)\rangle$  evolving according to the non-Hermitian effective Hamiltonian  $\mathcal{W}$  acting on a doubled Hilbert space. For any operator  $\mathcal{O}$ , we may compute the trace in the vectorized representation according to

$$\text{Tr}(\mathcal{O}\varrho) = \langle I | \mathcal{O} \otimes \mathbb{1} | \varrho \rangle, \quad (7)$$

where  $\langle I | = \sum_n \langle n | \otimes \langle n |$ . The eigenvalues of  $\mathcal{W}$ , which we denote by  $\{E_a\}$ , are related to those of the Liouvillian by  $E_a = -i\Lambda_a$ .

### C. Shibata-Katsura model

The SK model [3] describes a dissipative  $S = \frac{1}{2}$  chain. The Hamiltonian is

$$H = \sum_n (J_x X_{2n-1} X_{2n} + J_y Y_{2n} Y_{2n+1}) \quad (8)$$

and the jump operators are  $L_n = \sqrt{\gamma} Z_n$ , with  $\gamma > 0$ . Thus, we have

$$\begin{aligned} \mathcal{W}(\gamma) = & \sum_{n=1}^{N_c} (J_x X_{2n-1} X_{2n} + J_y Y_{2n} Y_{2n+1} - J_x \tilde{X}_{2n-1} \tilde{X}_{2n} \\ & - J_y \tilde{Y}_{2n} \tilde{Y}_{2n+1}) + i\gamma \sum_{j=1}^N (Z_j \tilde{Z}_j - 1), \end{aligned} \quad (9)$$

where the  $(X, Y, Z)$  operators act on the first Hilbert space and  $(\tilde{X}, \tilde{Y}, \tilde{Z})$  act on the copy. The system is depicted in Fig. 1 and corresponds to a non-Hermitian two-leg ladder.  $N_c$  is the number of unit cells, and there are  $N = 2N_c$  sites on each leg of the ladder. Note that  $\mathcal{W}^*(\gamma) = \mathcal{W}(-\gamma)$ , and that if we define  $R$  as the reflection operator mapping one leg into the other, i.e.,  $(X_j, Y_j, Z_j) \leftrightarrow (\tilde{X}_j, \tilde{Y}_j, \tilde{Z}_j)$  for all  $j$ , then

$$R \mathcal{W}(\gamma) R = -\mathcal{W}(-\gamma) = -\mathcal{W}^*(\gamma). \quad (10)$$

This establishes that the eigenvalues of  $\mathcal{W}(\gamma)$  come in pairs  $\Lambda_a^\pm = \pm E_a + i\Gamma_a$ . Total positivity requires that  $\text{Im}(\Gamma_a) \leq 0$ . Any NESS  $\varrho_{\text{NESS}}$  satisfies  $\mathcal{W}(\gamma) | \varrho_{\text{NESS}} \rangle = 0$ .

Introducing on each site four Majorana fermions  $\theta^{0,1,2,3}$  and expressing the Pauli matrices therefrom,

$$X_j = i\theta_j^0 \theta_j^1, \quad Y_j = i\theta_j^0 \theta_j^2, \quad Z_j = i\theta_j^0 \theta_j^3, \quad (11)$$

with corresponding expression for  $(\tilde{X}_j, \tilde{Y}_j, \tilde{Z}_j)$ , one may express  $\mathcal{W}(\gamma)$  as

$$\begin{aligned} \mathcal{W}(\gamma) = & \sum_{n=1}^{N_c} \{ iJ_x [\mu_{2n-1}^x \theta_{2n-1}^0 \theta_{2n}^0 - \tilde{\mu}_{2n-1}^x \tilde{\theta}_{2n-1}^0 \tilde{\theta}_{2n}^0] \\ & + iJ_y [\mu_{2n}^y \theta_{2n}^0 \theta_{2n+1}^0 - \tilde{\mu}_{2n}^y \tilde{\theta}_{2n}^0 \tilde{\theta}_{2n+1}^0] \} \\ & - \gamma \sum_{j=1}^N \mu_j^z \theta_j^0 \tilde{\theta}_j^0 - 2i\gamma N_c, \end{aligned} \quad (12)$$

where

$$\begin{aligned} \mu_{2n-1}^x &= -i\theta_{2n-1}^1 \theta_{2n}^1, & \tilde{\mu}_{2n-1}^x &= i\tilde{\theta}_{2n-1}^1 \tilde{\theta}_{2n}^1, \\ \mu_{2n}^y &= -i\theta_{2n}^2 \theta_{2n+1}^2, & \tilde{\mu}_{2n}^y &= -i\tilde{\theta}_{2n}^2 \tilde{\theta}_{2n+1}^2, & \mu_j^z &= -i\theta_j^3 \tilde{\theta}_j^3, \end{aligned} \quad (13)$$

are  $\mathbb{Z}_2$  gauge fields on the links of the two leg ladder in Fig. 1. These gauge fields commute with each other and with the  $\theta^0$  hopping terms, as well as with the constraints

$$\Lambda_j \equiv \theta_j^0 \theta_j^1 \theta_j^2 \theta_j^3 = +1, \quad \tilde{\Lambda}_j \equiv \tilde{\theta}_j^0 \tilde{\theta}_j^1 \tilde{\theta}_j^2 \tilde{\theta}_j^3 = +1, \quad (14)$$

which must be imposed at each site in order to guarantee  $XY = iZ$ . This is the magic of the Kitaev honeycomb lattice model, where the link lattice is also tripartite: The Hamiltonian corresponds to a single species ( $\theta^0$ ) of Majorana fermion hopping in the presence of a nondynamical  $\mathbb{Z}_2$  gauge field. The gauge-invariant content of the theory is contained in the plaquette fluxes  $\Phi_{2n-1} = \mu_{2n-1}^x \mu_{2n}^z \tilde{\mu}_{2n-1}^x \mu_{2n-1}^z$  and  $\Phi_{2n} = \mu_{2n}^y \mu_{2n+1}^z \tilde{\mu}_{2n}^y \mu_{2n}^z$  and in the Wilson phases  $Q = \prod_{j=1}^N Z_j$  and  $\tilde{Q} = \prod_{j=1}^N \tilde{Z}_j$ . With periodic boundary conditions,  $Q\tilde{Q} = \prod_{j=1}^N \Phi_j$ .

## III. DIRAC MATRIX SK MODEL

### A. Gamma matrix Kitaev models

A Clifford algebra is defined by the anticommutation relations,

$$\{\Gamma^a, \Gamma^b\} = 2\delta^{ab} \quad a, b \in \{1, \dots, n\}. \quad (15)$$

When  $n = 2k$ , a representation of the algebra can be constructed by tensor products of  $k$  Pauli matrices, viz.,

$$\begin{aligned} \Gamma^1 &= X \otimes \mathbb{1} \otimes \dots \otimes \mathbb{1} & \Gamma^{2k-1} &= Z \otimes Z \otimes \dots \otimes X \\ \Gamma^2 &= Y \otimes \mathbb{1} \otimes \dots \otimes \mathbb{1} & \Gamma^{2k} &= Z \otimes Z \otimes \dots \otimes Y \\ \Gamma^3 &= Z \otimes X \otimes \dots \otimes \mathbb{1} & \Gamma^{2k+1} &= Z \otimes Z \otimes \dots \otimes Z. \end{aligned} \quad (16)$$

The gamma matrices defined above are all Hermitian. In even dimensions, we define

$$\Gamma^{2k+1} = (-i)^k \Gamma^1 \Gamma^2 \dots \Gamma^{2k}. \quad (17)$$

Introducing  $2k + 2$  Majorana fermions  $\theta^a$  with indices  $a \in \{0, \dots, 2k + 1\}$  satisfying  $\{\theta^a, \theta^b\} = 2\delta^{ab}$ , we define  $\Gamma^\mu = i\theta^0 \theta^\mu$  with  $\mu > 0$ . Analogously to the constraint  $\theta^0 \theta^1 \theta^2 \theta^3 = 1$  when  $k = 1$ , we demand

$$\theta^0 \theta^1 \dots \theta^{2k+1} = i^{k-1}. \quad (18)$$

The case  $k = 1$  yields the  $2 \times 2$  Pauli matrices, with  $\Gamma^1 = X$ ,  $\Gamma^2 = Y$ , and  $\Gamma^3 = -i\Gamma^1 \Gamma^2 = Z$ . The case  $k = 2$  yields

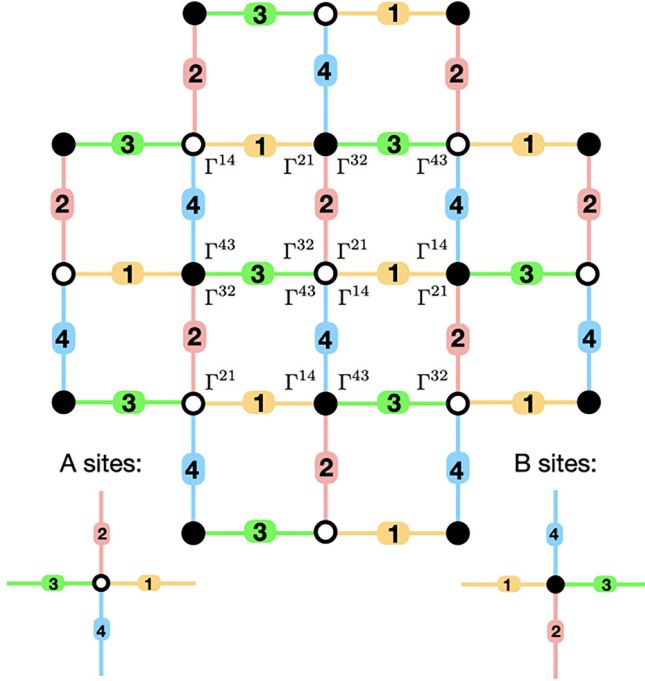


FIG. 2. Square lattice Dirac matrix Shibata-Katsura model. See description in Sec. III B.

the  $4 \times 4$  Dirac matrices, with  $\Gamma^5 = -\Gamma^1\Gamma^2\Gamma^3\Gamma^4$ . For general  $k$  this yields  $2k + 1$  matrices of rank  $2^k$ . One can then form  $\Gamma^{\mu\nu} = i\Gamma^\mu\Gamma^\nu = i\theta^\mu\theta^\nu$  of which there are  $\binom{2k+1}{2}$  independent representatives (take  $\mu < \nu$ ), and next  $\Gamma^{\mu\nu\rho} = -i\Gamma^\mu\Gamma^\nu\Gamma^\rho = \theta^0\theta^\mu\theta^\nu\theta^\rho$  and  $\Gamma^{\mu\nu\rho\sigma} = \theta^\mu\theta^\nu\theta^\rho\theta^\sigma$ , which yield  $\binom{2k+1}{3}$  and  $\binom{2k+1}{4}$  independent terms, respectively. Proceeding thusly, one obtains at level  $k$  a basis of  $4^k$  Hermitian matrices of rank  $2^k$ .

Analogs of Kitaev's honeycomb lattice model using these higher-level Clifford algebras have been considered, *inter alia* in Refs. [7,8], with interactions  $\Gamma_i^\mu\Gamma_j^\mu$  along the links. When the underlying lattice is such that each site lies at the confluence of  $2k + 1$  distinctly labeled  $\mu$  links, the “spin” Hamiltonian is again expressible as a single species ( $\theta^0$ ) Majorana fermion hopping in the presence of a static  $\mathbb{Z}_2$  gauge field. Other generalizations, in which multiple species of Majoranas hop in the same  $\mathbb{Z}_2$  static gauge field and hybridize as well have also been constructed [7,14].

### B. Dirac matrix SK model

We generalize the SK model to a dissipative  $\Gamma$ -matrix model defined on the square lattice, as depicted in Fig. 2. We regard the square lattice as bipartite, with elementary direct lattice vectors  $\mathbf{a}_{1,2} = \hat{x} \pm \hat{y}$ . Our Hamiltonian is

$$H = \sum_{\mathbf{R}} (J_1 \Gamma_{\mathbf{R}}^1 \Gamma_{\mathbf{R}+\hat{x}}^1 + J_2 \Gamma_{\mathbf{R}}^2 \Gamma_{\mathbf{R}+\hat{y}}^2 + J_3 \Gamma_{\mathbf{R}}^3 \Gamma_{\mathbf{R}-\hat{x}}^3 + J_4 \Gamma_{\mathbf{R}}^4 \Gamma_{\mathbf{R}-\hat{y}}^4), \quad (19)$$

where  $\mathbf{R} = n_1\mathbf{a}_1 + n_2\mathbf{a}_2$  with  $n_{1,2} \in \mathbb{Z}$  are the A sublattice sites, which are  $N_c$  in number. We use the symbol  $\mathbf{r}$  to denote a site which may be in either sublattice. Thus, on each site of

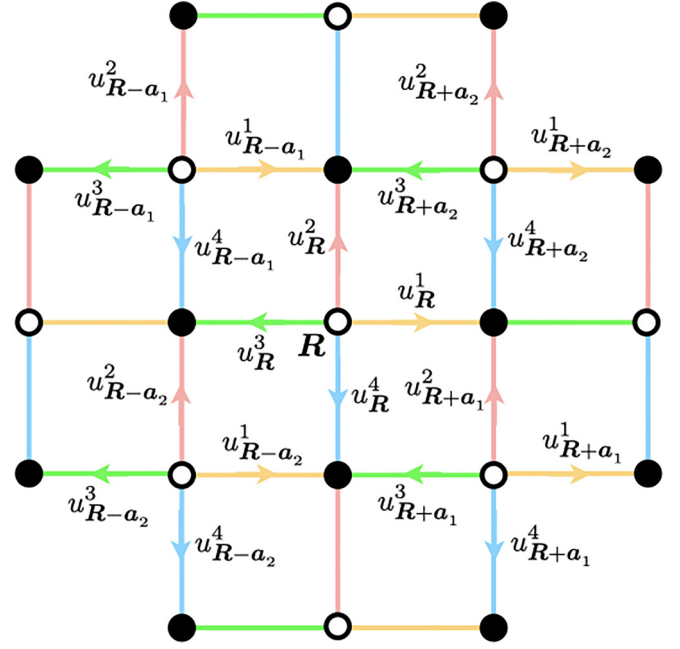


FIG. 3. At each A sublattice site in the bottom layer, the gauge field  $u_{\mathbf{R}}^\delta$  points along the nearest-neighbor vector  $\delta$  toward a neighboring B sublattice site. A corresponding convention pertains for the  $\tilde{u}_{\mathbf{R}}^\delta$  gauge fields in the top layer.

the square lattice, a four-dimensional Hilbert space is acted on by operators  $1_r$ ,  $\Gamma_r^\mu$ , and  $\Gamma_r^{\mu\nu}$ , where  $\Gamma^\mu$  are  $4 \times 4$  Dirac matrices, with  $\mu \in \{1, \dots, 5\}$ .

Following SK, we take the Lindblad jump operators to be  $L_r = \sqrt{\gamma} \Gamma_r^5$  at each site. The GKLS master equation can then be written as a non-Hermitian Hamiltonian evolution of a model on a square lattice bilayer, with each layer corresponding to one copy of the Hilbert space. This Hamiltonian is

$$\mathcal{W}(\{J_\delta\}, \gamma) = \sum_{\mathbf{R} \in \mathbf{A}} \sum_{\delta=1}^4 J_\delta \left( iu_{\mathbf{R}}^\delta \theta_{\mathbf{R}}^0 \theta_{\mathbf{R}+\delta}^0 - i\tilde{u}_{\mathbf{R}}^\delta \tilde{\theta}_{\mathbf{R}}^0 \tilde{\theta}_{\mathbf{R}+\delta}^0 \right) - \gamma \sum_{\mathbf{r} \in \mathbf{A}, \mathbf{B}} u_{\mathbf{r}}^5 \theta_{\mathbf{r}}^0 \tilde{\theta}_{\mathbf{r}}^0 - 2i\gamma N_c, \quad (20)$$

where  $\delta \in \{\hat{x}, \hat{y}, -\hat{x}, -\hat{y}\}$  for  $\delta \in \{1, 2, 3, 4\}$ , respectively, and where (see Fig. 3)

$$u_{\mathbf{R}}^\delta = -i\theta_{\mathbf{R}}^\delta \theta_{\mathbf{R}+\delta}^\delta, \quad \tilde{u}_{\mathbf{R}}^\delta = -i\tilde{\theta}_{\mathbf{R}}^\delta \tilde{\theta}_{\mathbf{R}+\delta}^\delta, \quad u_{\mathbf{r}}^5 = -i\theta_{\mathbf{r}}^5 \tilde{\theta}_{\mathbf{r}}^5, \quad (21)$$

are the nondynamical gauge fields in the bottom, top, and between layer regions. There are  $5N$  such gauge fields, but as we shall see the number of gauge-invariant quantities is  $3N + 1$ , i.e., there are  $2^{3N+1}$  gauge sectors, where  $N$  is the total number of sites in either layer. Similar considerations which led to Eq. (10) in the SK model hold for our model as well, hence the eigenvalues of  $\mathcal{W}(\gamma)$  come in pairs  $\Lambda_a^\pm = \pm E_a + i\Gamma_a$ , with  $\text{Im}(\Gamma_a) \leq 0$ .

#### 1. Conserved quantities

For the original SK model, the product  $Q = Z_1 \cdots Z_N$  is conserved as it commutes with  $H$  and with each of the jump operators  $\sqrt{\gamma} Z_j$ . This means that both  $\mathbb{1}$  and  $Q$  are annihilated



by the Liouvillian  $\mathcal{L}$ , and that both

$$\varrho_{\pm} = 2^{-N}(\mathbb{1} \pm \mathcal{Q}) \quad (22)$$

are thus valid NESS, for all  $\gamma$  [3].

For our model of Eq. (20), there are vastly more conserved quantities. With periodic boundary conditions along both axes, there are  $N + 1$  gauge-invariant quantities, which are the  $N$  plaquette fluxes (see Fig. 2),

$$\Phi_r \equiv \begin{cases} -\Gamma_r^{21} \Gamma_{r+\hat{x}}^{14} \Gamma_{r+\hat{x}+\hat{y}}^{43} \Gamma_{r+\hat{y}}^{32} & \text{if } r \in \text{A} \\ -\Gamma_r^{43} \Gamma_{r+\hat{x}}^{32} \Gamma_{r+\hat{x}+\hat{y}}^{21} \Gamma_{r+\hat{y}}^{14} & \text{if } r \in \text{B} \end{cases}, \quad (23)$$

where the  $\mathbb{Z}_2$  flux in plaquette  $r$  is labeled by the lower left site of the plaquette [15]. Note that the product  $\prod_r \Phi_r = 1$ , and hence there are  $N - 1$  independent  $\mathbb{Z}_2$  plaquette fluxes. In addition, we have the two Wilson phases,

$$\begin{aligned} W_x &= -\Gamma_{1,1}^{13} \Gamma_{2,1}^{31} \cdots \Gamma_{N_x-1,1}^{13} \Gamma_{N_x,1}^{31} \\ W_y &= -\Gamma_{1,1}^{24} \Gamma_{1,2}^{42} \cdots \Gamma_{1,N_y-1}^{24} \Gamma_{1,N_y}^{42}, \end{aligned} \quad (24)$$

where both  $N_x$  and  $N_y$  are taken to be even, and with the total number of sites  $N \equiv N_x N_y$ . (Note that  $\Gamma^{31} = -\Gamma^{13}$  and  $\Gamma^{42} = -\Gamma^{24}$ ; we choose to write the Wilson phases as above because the repetition of consecutive  $\Gamma$ -matrix indices is a useful mnemonic.) One can readily check that  $\Phi_r$  commutes with both  $H$  and with all the jump operators. In addition, the operator  $\mathcal{Q} = \prod_r \Gamma_r^5$  also commutes with the Hamiltonian and with all of the jump operators. However, if we examine the product of the  $\mathbb{Z}_2$  fluxes over the  $\text{A}$  plaquettes alone, i.e., over those plaquettes with an  $\text{A}$  site in their lower left corner, then from  $\Gamma^{43} \Gamma^{21} = -\Gamma^1 \Gamma^2 \Gamma^3 \Gamma^4 = \Gamma^5$ , we conclude that  $\prod_{R \in \text{A}} \phi_R = \prod_r \Gamma_r^5 = \mathcal{Q}$ , and therefore  $\mathcal{Q}$  is not an independent conserved quantity. Finally, as the jump operators are all normal, according to Eq. 2 we have a  $2^{N+1}$ -dimensional subspace of  $T = \infty$  nonequilibrium steady states, since there are  $2^{N+1}$  projectors,

$$\Pi_{\eta_x, \eta_y, \{\eta_r\}} \equiv \left( \frac{1 + \eta_x W_x}{2} \right) \left( \frac{1 + \eta_y W_y}{2} \right) \prod_r' \left( \frac{1 + \eta_r \phi_r}{2} \right), \quad (25)$$

labeled by  $\eta_x, \eta_y$ , and  $\{\eta_r\}$ , each taking the value  $\pm 1$ , which commute with  $H$  and with all the jump operators  $L_r$ . The prime on the product indicates that the final plaquette with  $r = (N_x, N_y)$  is omitted. The total number of unnormalized density matrices is  $(4^2)^N = 16^N$ . That is, any density matrix of the form

$$\varrho = \sum_{\eta_x} \sum_{\eta_y} \sum_{\{\eta_r\}} C_{\eta_x, \eta_y, \{\eta_r\}} \Pi_{\eta_x, \eta_y, \{\eta_r\}} \quad (26)$$

with  $\text{Tr} \varrho = \sum_{\eta_x} \sum_{\eta_y} \sum_{\{\eta_r\}} C_{\eta_x, \eta_y, \{\eta_r\}} = 1$  and each  $C_{\eta_x, \eta_y, \{\eta_r\}} \geq 0$  is a valid NESS.

### C. Analysis

We define a complex fermion living along each link between planes of the bilayer, *viz.*,

$$c_r = \frac{1}{2}(\theta_r^0 + i\tilde{\theta}_r^0), \quad c_r^\dagger = \frac{1}{2}(\theta_r^0 - i\tilde{\theta}_r^0), \quad (27)$$

and thus

$$\theta_r^0 = c_r^\dagger + c_r, \quad \tilde{\theta}_r^0 = i(c_r^\dagger - c_r). \quad (28)$$

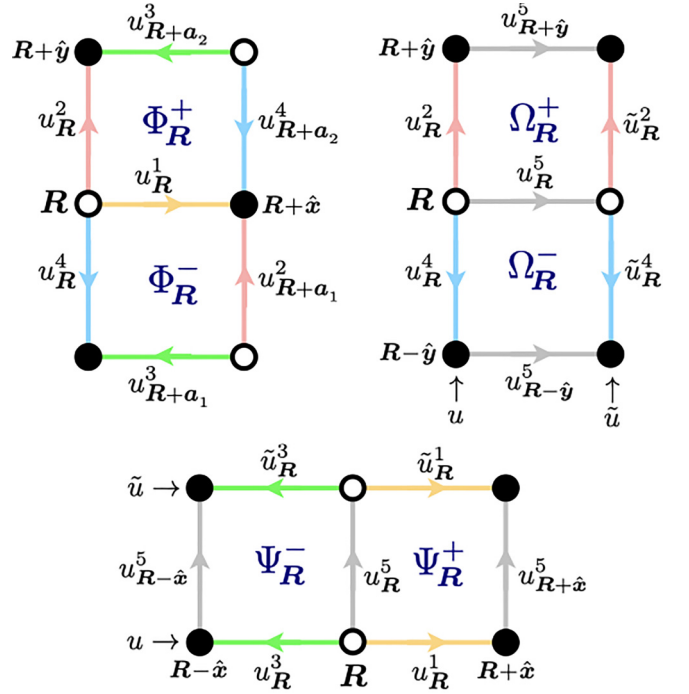


FIG. 4. Associated with each  $\text{A}$  sublattice site in the bottom layer are eight square plaquette fluxes:  $\Phi_R^\pm$ ,  $\tilde{\Phi}_R^\pm$  (not shown),  $\Psi_R^\pm$ , and  $\Omega_R^\pm$ .

The non-Hermitian Hamiltonian of Eq. (20) is then expressed in terms of these complex fermions as

$$\begin{aligned} \mathcal{W} &= \sum_{R \in \text{A}} \sum_{\delta=1}^4 \{ iJ_\delta (u_R^\delta - \tilde{u}_R^\delta) (c_R^\dagger c_{R+\delta} + c_{R+\delta}^\dagger c_R) \\ &\quad + iJ_\delta (u_R^\delta + \tilde{u}_R^\delta) (c_R^\dagger c_{R+\delta}^\dagger - c_{R+\delta} c_R) \} \\ &\quad + i\gamma \sum_{r \in \text{A, B}} u_r^5 (2c_r^\dagger c_r - 1) - 2iN_c \gamma. \end{aligned} \quad (29)$$

### D. Counting degrees of freedom

Associated with each  $\text{A}$  sublattice site in the bottom layer are eight square plaquette  $\mathbb{Z}_2$  fluxes (see Fig. 4). These fall into three groups. First are the fluxes through the  $(x, y)$  plaquettes. For the bottom layer we have

$$\begin{aligned} \Phi_R^+ &= u_R^1 u_{R+a_2}^4 u_{R+a_2}^3 u_R^2 = -\Gamma_R^{21} \Gamma_{R+\hat{x}}^{14} \Gamma_{R+a_2}^{43} \Gamma_{R+\hat{y}}^{32} \\ \Phi_R^- &= u_R^4 u_{R+a_1}^3 u_{R+a_1}^2 u_R^1 = -\Gamma_R^{14} \Gamma_{R-\hat{y}}^{43} \Gamma_{R+a_1}^{32} \Gamma_{R+\hat{x}}^{21}, \end{aligned} \quad (30)$$

with corresponding expressions involving  $\tilde{\Phi}_R^\pm$ ,  $\tilde{\Gamma}_r$ , and  $\tilde{u}_R^\delta$  in the top layer. Next, the  $(x, z)$  plaquette fluxes  $\Psi_R^\pm$ ,

$$\begin{aligned} \Psi_R^+ &= u_R^1 u_{R+\hat{x}}^5 \tilde{u}_R^1 u_R^5 = -\Gamma_R^{51} \Gamma_{R+\hat{x}}^{15} \tilde{\Gamma}_{R+\hat{x}}^{51} \tilde{\Gamma}_R^{15} \\ \Psi_R^- &= u_R^5 \tilde{u}_R^3 u_{R-\hat{x}}^5 u_R^3 = -\Gamma_R^{35} \Gamma_R^{53} \tilde{\Gamma}_{R-\hat{x}}^{35} \tilde{\Gamma}_{R-\hat{x}}^{53}. \end{aligned} \quad (31)$$

Finally, the  $(y, z)$  plaquette fluxes  $\Omega_R^\pm$  are given by

$$\begin{aligned}\Omega_R^+ &= u_R^2 u_{R+y}^5 \tilde{u}_R^2 u_R^5 = -\Gamma_R^{52} \Gamma_{R+y}^{25} \tilde{\Gamma}_{R+y}^{52} \tilde{\Gamma}_R^{25} \\ \Omega_R^- &= u_R^5 \tilde{u}_R^4 u_{R-y}^5 u_R^4 = -\Gamma_R^{45} \tilde{\Gamma}_R^{54} \tilde{\Gamma}_{R-y}^{45} \Gamma_{R-y}^{54}.\end{aligned}\quad (32)$$

There are also the Wilson phases,

$$\begin{aligned}W_x &= u_{1,1}^1 (-u_{3,1}^3) u_{3,1}^1 (-u_{5,1}^5) \cdots u_{N_x-1,1}^1 (-u_{1,1}^3) \\ &= -\Gamma_{1,1}^{13} \Gamma_{2,1}^{31} \cdots \Gamma_{N_x,1}^{31} \\ W_y &= u_{1,1}^2 (-u_{1,3}^4) u_{1,3}^2 (-u_{1,5}^4) \cdots u_{1,N_y-1}^2 (-u_{1,1}^4) \\ &= \Gamma_{1,1}^{24} \Gamma_{1,2}^{42} \cdots \Gamma_{1,N_y}^{42},\end{aligned}\quad (33)$$

again with corresponding expressions for  $\tilde{W}_x$  and  $\tilde{W}_y$ . At this point it appears that we have  $4N + 4$  gauge-invariant  $\mathbb{Z}_2$  degrees of freedom. However, the total flux through each of the  $N$  cubes must be trivial, providing  $N$  constraints. There is an additional constraint  $\prod_R \Phi_R^+ \Phi_R^- = 1$  due to periodic boundary conditions; the corresponding expression in the top layer does not yield new information given the condition on each of the cubes. Finally, there are two constraints relating the products of the Wilson phases in each of the layers to the  $\Omega$  and  $\Psi$  plaquette fluxes [see Eq. (41) below]. Thus, there are  $N + 3$  independent constraints, and therefore  $3N + 1$  independent gauge-invariant configurations of the fluxes and Wilson phases. We must also acknowledge the constraints imposed by the projectors which enforce  $\Lambda_r = \tilde{\Lambda}_r = 1$ , with  $\Lambda_r = \theta_r^0 \theta_r^1 \theta_r^2 \theta_r^3 \theta_r^4 \theta_r^5 = -i$ . Taking the product over all sites, we obtain [7]

$$\prod_r i \theta_r^0 \tilde{\theta}_r^0 \times \prod_{R,\delta} u_R^\delta \tilde{u}_R^\delta \times \prod_r u_r^5 = 1. \quad (34)$$

This expression includes a product over all the itinerant fermion parities  $2c_r^\dagger c_r - 1$  as well as over each of the  $5N\mathbb{Z}_2$  gauge fields which reside on the links of the bilayer structure. It thereby constrains the parity of the  $c$ -fermions, which are constructed from  $\theta^0$  and  $\tilde{\theta}^0$  on each of the interplane links. Thus rather than  $N$  freedoms for the dynamical fermion states, there are  $N - 1$ , and the total number of states in our doubled Hilbert space is  $2^{3N+1} \times 2^{N-1} = 16^N$ , which is the correct number of density matrices for an  $N$ -site system described by  $4 \times 4$  gamma matrices [16].

### E. Choosing a gauge

Given the  $3N + 1$  independent plaquette fluxes and Wilson phases, how can we pick a gauge? Let us first consider the planar fluxes  $\Phi_R^\pm$  in the bottom layer and the sketch in Fig. 5. The coordinates of the **A** sublattice site in the lower left corner are  $\mathbf{r} = (x, y) = (1, 1)$ . The Wilson phase fluxes are defined to be  $u_{1,1}^1 \equiv W_x$  and  $u_{1,1}^4 \equiv -W_y$ . We then define the remaining unassigned gauge fields as follows:

$$\begin{aligned}u_{2,2}^3 &= \Phi_{1,1}^+ u_{1,1}^1 & u_{2,2}^1 &= \Phi_{2,2}^- \\ u_{1,3}^1 &= \Phi_{1,3}^- u_{2,2}^3 & u_{3,3}^3 &= \Phi_{2,2}^+ u_{2,2}^1 \quad \dots \\ u_{1,N_y-1}^1 &= \Phi_{1,N_y-1}^- u_{2,N_y-2}^3 & u_{3,N_y-1}^3 &= \Phi_{2,N_y-2}^+ u_{2,N_y-2}^1 \\ u_{2,N_y}^3 &= \Phi_{1,N_y-1}^+ u_{1,N_y-1}^1 & u_{2,N_y}^1 &= \Phi_{2,N_y}^- u_{3,N_y-1}^3 \\ u_{2,N_y}^2 &= \Phi_{1,1}^- u_{1,1}^4 u_{2,N_y}^3 & u_{3,1}^4 &= \Phi_{2,N_y}^- u_{2,N_y}^1 u_{2,N_y}^2\end{aligned}$$

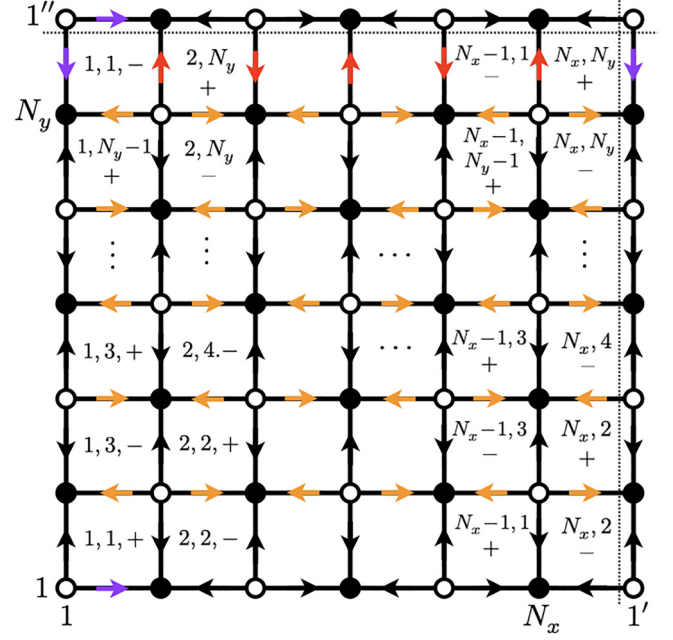


FIG. 5. Labels of the unit cells  $\Phi_R^\pm$ . The black arrows indicate  $u_r^\delta = +1$  in the direction of the arrow. There are  $N + 1$  colored arrows, which are determined by the  $N - 1$  independent plaquette fluxes and the two Wilson loops. A corresponding assignment pertains to the upper layer with fluxes  $\tilde{\Phi}_R^\pm$  and gauge fields  $\tilde{u}_r^\delta$ . Dotted lines indicate periodicity boundaries.

and

$$\begin{aligned}u_{4,2}^3 &= \Phi_{3,1}^+ & u_{N_x,2}^1 &= \Phi_{N_x,2}^- \\ u_{3,3}^1 &= \Phi_{3,3}^- u_{4,2}^3 & u_{1,3}^3 &= \Phi_{N_x,2}^+ u_{N_x,2}^1 \\ u_{3,4}^3 &= \Phi_{3,3}^+ u_{3,3}^1 & u_{1,4}^1 &= \Phi_{N_x,4}^- u_{1,3}^3 \quad \dots \\ u_{3,N_y-1}^1 &= \Phi_{3,N_y-1}^- u_{4,N_y-2}^3 & u_{1,N_y-1}^3 &= \Phi_{N_x,N_y-2}^+ u_{N_x,N_y-2}^1 \\ u_{4,4}^3 &= \Phi_{3,N_y-1}^+ u_{3,N_y-1}^1 & u_{1,N_y}^1 &= \Phi_{N_x,N_y}^- u_{1,3}^3 \\ u_{3,1}^4 &= \Phi_{2,N_y}^+ u_{2,N_y}^3 u_{2,N_y}^1 & u_{1,1}^4 &= -W_y.\end{aligned}\quad (35)$$

Thus, we can iteratively obtain all the unassigned  $\mathbb{Z}_2$  gauge fields  $u_r^\delta$  from the plaquette phases and the Wilson phases. Again, corresponding expressions hold in the upper layer for the quantities  $\{\tilde{u}_r^\delta, \tilde{\Phi}_R^\pm, \tilde{W}_x, \tilde{W}_y\}$ .

Next, we consider the  $u_R^5$  gauge fields and the plaquette fluxes  $\{\Psi_R^\pm, \Omega_R^\pm\}$ . From Eq. (30) we may iteratively determine the values of the  $u_{m,k}^5$  for odd values of  $k$  given the value  $u_{1,k}^5 \equiv 1$ :

$$\begin{aligned}u_{2,k}^5 &= u_{1,k}^1 \tilde{u}_{1,k}^1 \Psi_{1,k}^+ \cdot u_{1,k}^5 \\ u_{3,k}^5 &= u_{3,k}^3 \tilde{u}_{3,k}^3 \Psi_{3,k}^- \cdot u_{2,k}^5 \\ u_{4,k}^5 &= u_{3,k}^1 \tilde{u}_{3,k}^1 \Psi_{3,k}^+ \cdot u_{3,k}^5 \quad \dots \\ u_{N_x,k}^5 &= u_{N_x-1,k}^1 \tilde{u}_{N_x-1,k}^1 \Psi_{N_x-1,k}^+ \cdot u_{N_x-1,k}^5 \\ u_{1,k}^5 &= u_{1,k}^1 \tilde{u}_{1,k}^1 \Psi_{1,k}^- \cdot u_{N_x,k}^5.\end{aligned}\quad (36)$$

For even values of  $k$ , we have

$$\begin{aligned}
u_{2,k}^5 &= u_{2,k}^3 \tilde{u}_{2,k}^3 \Psi_{2,k}^- \cdot u_{1,k}^5 \\
u_{3,k}^5 &= u_{2,k}^1 \tilde{u}_{2,k}^1 \Psi_{2,k}^+ \cdot u_{2,k}^5 \\
u_{4,k}^5 &= u_{4,k}^3 \tilde{u}_{4,k}^3 \Psi_{4,k}^- \cdot u_{3,k}^5 \quad \dots \\
u_{N_x,k}^5 &= u_{N_x,k}^3 \tilde{u}_{N_x,k}^3 \Psi_{N_x,k}^- \cdot u_{N_x-1,k}^5 \\
u_{1,k}^5 &= u_{N_x,k}^1 \tilde{u}_{N_x,k}^1 \Psi_{N_x,k}^+ \cdot u_{N_x,k}^5.
\end{aligned} \tag{37}$$

To obtain  $u_{1,k+1}^5$  from  $u_{1,k}^5$ , we use the relations

$$\begin{aligned}
u_{1,2n}^5 &= u_{1,2n-1}^2 \tilde{u}_{1,2n-1}^2 \Omega_{1,2n-1}^+ \cdot u_{1,2n-1}^5 \\
u_{1,2n+1}^5 &= u_{1,2n}^4 \tilde{u}_{1,2n}^4 \Omega_{1,2n+1}^- \cdot u_{1,2n}^5.
\end{aligned} \tag{38}$$

Equations (36), (37), and (38) entail the relations

$$\begin{aligned}
\prod_{\substack{j=1 \\ (k \text{ odd})}}^{N_x} \Psi_{j,k}^- \Psi_{j,k}^+ &= \prod_{m=1}^{N_x/2} u_{2m-1,k}^1 u_{2m-1,k}^3 \tilde{u}_{2m-1,k}^1 \tilde{u}_{2m-1,k}^3 \\
\prod_{\substack{j=1 \\ (k \text{ even})}}^{N_x} \Psi_{j,k}^- \Psi_{j,k}^+ &= \prod_{m=1}^{N_x/2} u_{2m,k}^1 u_{2m,k}^3 \tilde{u}_{2m,k}^1 \tilde{u}_{2m,k}^3,
\end{aligned} \tag{39}$$

for  $k$  odd and even, respectively, as well as

$$\begin{aligned}
\prod_{\substack{k=1 \\ (j \text{ odd})}}^{N_y} \Omega_{j,k}^- \Omega_{j,k}^+ &= \prod_{n=1}^{N_y/2} u_{j,2n-1}^2 u_{j,2n-1}^4 \tilde{u}_{j,2n-1}^2 \tilde{u}_{j,2n-1}^4 \\
\prod_{\substack{k=1 \\ (j \text{ even})}}^{N_y} \Omega_{j,k}^- \Omega_{j,k}^+ &= \prod_{n=1}^{N_y/2} u_{j,2n}^2 u_{j,2n}^4 \tilde{u}_{j,2n}^2 \tilde{u}_{j,2n}^4,
\end{aligned} \tag{40}$$

for  $j$  odd and even, respectively. Restricting to the cases  $j = 1$  and  $k = 1$ , we can relate these products to the Wilson phases in Eq. (33), *viz.*,

$$\begin{aligned}
\prod_{k=1}^{N_y} \Omega_{1,k}^- \Omega_{1,k}^+ &= W_x \tilde{W}_x \\
\prod_{j=1}^{N_x} \Psi_{j,1}^- \Psi_{j,1}^+ &= W_y \tilde{W}_y.
\end{aligned} \tag{41}$$

We showed previously in Sec. III D that, considering all the  $\mathbb{Z}_2$  gauge degrees of freedom, we have a total of  $3N + 1$  independent plaquette fluxes and Wilson phases. In each layer, there are  $N + 1$  free gauge fields  $u_{\mathbf{R}}^\delta$ , as depicted in Fig. 5. Between the layers, there are  $N - 1$  free gauge fields  $u_r^5$ , with  $u_{1,1}^5 \equiv 1$ . Thus, our gauge assignment accounts for all the independent gauge-invariant quantities.

### F. Counting the NESS

Referring to Eq. (29), in order to obtain an eigenvalue of zero, we must have each  $u_r^5 = +1$  and  $c_r^\dagger c_r = 1$ . [The case  $u_r^5 = -1$  for all  $r$  is impossible since we have, without loss of generality (i.e., up to a gauge transformation), set  $u_{1,1}^5 \equiv 1$ .] We then must eliminate the BCS pairing terms, which would allow for the simultaneous annihilation of two neighboring  $c$ -fermions. This is accomplished by setting  $u_{\mathbf{R}}^\delta + \tilde{u}_{\mathbf{R}}^\delta = 0$  for

all  $\mathbf{R}$  and  $\delta$ . While this may seem inconsistent with the assignment of the fixed gauge fields (black arrows) in the two layers as depicted in Fig. 5, in fact we are free to redefine  $\tilde{u}_{\mathbf{R}}^\delta \rightarrow -\tilde{u}_{\mathbf{R}}^\delta$  for the purposes of counting the NESS. Thus, there are a total of  $N + 1$  independent values of the planar ( $\delta \in \{1, 2, 3, 4\}$ ) gauge fields associated with the NESS block, and therefore  $2^{N+1}$  degenerate NESS.

It can be seen that for these NESS  $\Phi_{\mathbf{R}}^+ = \tilde{\Phi}_{\mathbf{R}}^+$  and  $\Phi_{\mathbf{R}}^- = \tilde{\Phi}_{\mathbf{R}}^-$ , as well as  $\Psi_{\mathbf{R}}^+ = \Psi_{\mathbf{R}}^- = -1$  and  $\Omega_{\mathbf{R}}^+ = \Omega_{\mathbf{R}}^- = -1$ , for all  $\mathbf{R}$ . Since  $\prod_{\mathbf{R}} \Phi_{\mathbf{R}}^+ \Phi_{\mathbf{R}}^- = 1$ , this accounts for  $N - 1$  freedoms associated with the plaquette fluxes. The Wilson phases  $W_x$  and  $W_y$  are also free [but  $\tilde{W}_x$  and  $\tilde{W}_y$  are then fixed by Eq. (41)], and so again we see that there are  $2^{N+1}$  NESS.

We numerically verified this counting for the case  $N_x = N_y = 2$  ( $N = 4$ ) by choosing the  $J_\delta$  couplings to be all different. However, when  $J_1 = J_2 = J_3 = J_4$  there is an enlarged translational symmetry, and we find a degeneracy of 162 (see Appendix A for details on constraints and our understanding of their implementations in the calculations) rather than  $2^{N+1} = 32$ . We also find that these additional degenerate states do not satisfy the flux conditions described in the previous paragraph.

## IV. COMPUTATIONAL RESULTS

To calculate the spectrum within a given gauge sector, we use Prosen's method for complex antisymmetric matrices [2]. Implementing the field assignments mentioned in section III E, we calculate the Liouvillian gap  $g$  to the smallest relaxation rate, i.e., the negative of the real part of the eigenvalues of  $\mathcal{L}$ , by searching over all the sectors of the  $\mathcal{L}$  corresponding to the different plaquette flux and Wilson phase configurations, for the case  $N_x = N_y = 2$ . For this system there are  $N = 4$  sites and thus  $2^{16}$  (unnormalized) density matrices. We perform calculations to identify two classes of gaps—one corresponding to an even sum of occupation numbers and one corresponding to an odd sum of occupation numbers in Prosen's Bogoliubov transformation, which we henceforth refer to as  $f$  parity (see Appendix A). We find that the gap corresponding to the even sum is smaller than the gap corresponding to the odd sum. We observe a transition in the first decay modes for the case with the even sum. The plot showing  $g$  as a function of  $\gamma$  for  $J_1 = J_2 = J_3 = J_4 = 1$  is shown in Fig. 6 (even sum) and Fig. 7 (odd sum). The gauge-invariant quantities corresponding to the first decay modes for the even sum calculation are shown in Figs. 8 and 9.

The results obtained from  $N_x = N_y = 2$  system could be subject to finite-size effects. Hence we proceed to estimate the gap for higher system sizes, using other methods to optimize for the gap since it is computationally intensive to examine all  $2^{3N+1}$  of the gauge sectors. We first tried looking at all configurations with a fixed number  $N_v$  of  $\mathbb{Z}_2$  defects—plaquettes and Wilson phases whose values are reversed relative to a given NESS configuration. (A reversed-flux plaquette is a  $\mathbb{Z}_2$  vortex.) There being  $N_g = 3N + 1$  gauge degrees of freedom, the number of such configurations  $\binom{N_g}{N_v}$  rapidly becomes computationally unwieldy with growing  $N_g$  and  $N_v$ . We searched exhaustively for the smallest nonzero relaxation rates for up to  $N_v = 4$  total  $\mathbb{Z}_2$  defects for  $N_x = N_y = 4$  and only up to

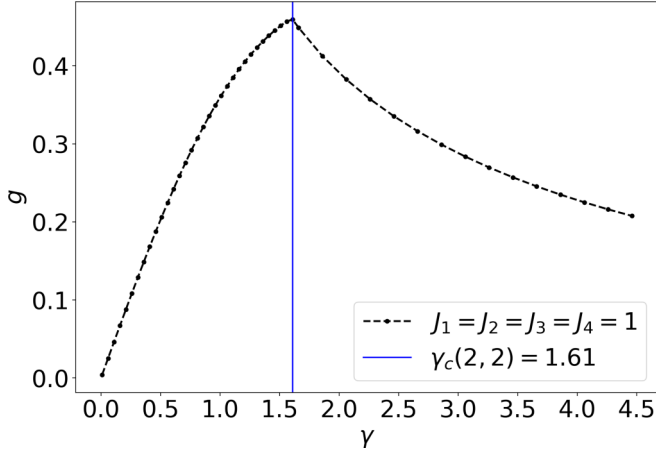


FIG. 6. Liouvillian gap  $g$  versus dissipator strength  $\gamma$  in the two-dimensional generalized SK model with periodic boundary conditions for  $N_x = N_y = 2$  and all  $J_\delta = 1$ . The  $f$  parity is fixed to be even. There is a transition in the first decay modes at the cusp seen at  $\gamma = \gamma_c(2, 2)$ , depicted by the blue vertical line.

$N_v = 2$  for  $N_x = N_y = 6$  relative to a particular NESS (one with all gauge-invariant  $\mathbb{Z}_2$  data set to  $-1$ ). We also performed Monte Carlo searches using both simulated annealing (SA) and a genetic algorithm (GA) capable of finding states with arbitrary numbers of defects. These both yielded similar results, and below we show data only for simulated annealing computations when comparing with the  $N_v$ -limited searches.

Some details regarding SA and the GA are provided in Sec. C below. We found the results obtained from SA to be satisfactory both in terms of convergence of the longest nonzero relaxation rate  $g$  as well as the computational run time for systems up to size  $6 \times 6$  ( $2^{144}$  density matrices). We cannot estimate the full spectrum of first decay modes through this method, i.e., enumerating all their degeneracies as in the  $2 \times 2$  case, or claim that it is definitively the first decay mode, however. The results obtained by taking the minimum value

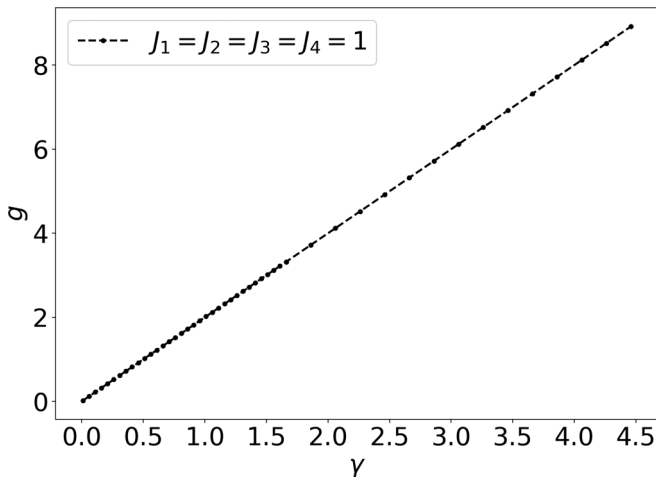


FIG. 7. Liouvillian gap  $g$  versus dissipator strength  $\gamma$  in the two-dimensional generalized SK model with periodic boundary conditions for  $N_x = N_y = 2$  and all  $J_\delta = 1$ . The  $f$  parity is fixed to be odd. We observe a change in the number of first decay modes at the following values of  $\gamma$ : 1.31, 1.61, 2.66, and 3.26.

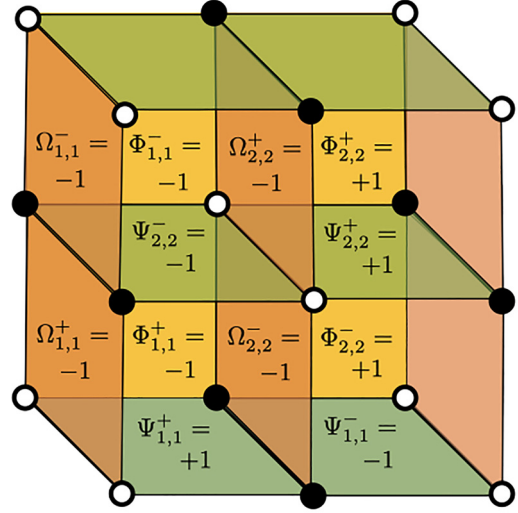


FIG. 8. A first decay mode of the two-dimensional generalized SK model with periodic boundary conditions for  $N_x = N_y = 2$  and  $J_1 = J_2 = J_3 = J_4 = 1$  corresponding to the “phase” where  $\gamma \leq \gamma_c(2, 2)$ . For the mode shown in this figure, we have  $W_x = 1, W_y = -1, \tilde{W}_x = -1, \tilde{W}_y = -1$ . There are 15 other configurations of the flux plaquettes and Wilson phases corresponding to the same eigenvalue as the first decay mode shown here.

from different runs (see Sec. C) of SA are shown in Fig. 10 and Fig. 11. The result for  $N_x = N_y = 6$  is subject to more error since we used a fewer number of runs than in the  $4 \times 4$  case. This estimate can be improved by using the decay modes obtained from SA.

To obtain better estimates, we collect the best configurations (i.e., those with the lowest relaxation rates) from

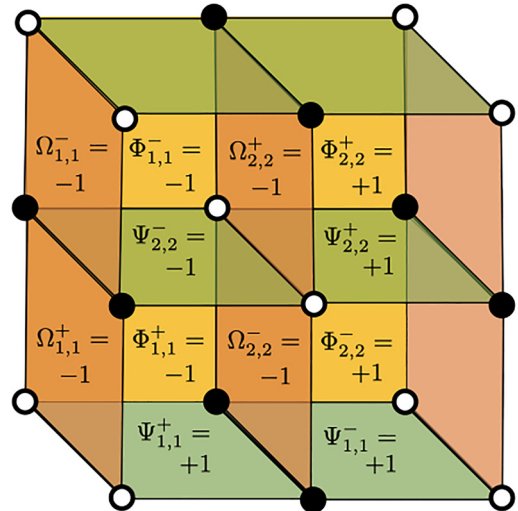


FIG. 9. A first decay mode of the two-dimensional generalized SK model with periodic boundary conditions for  $N_x = N_y = 2$  and  $J_1 = J_2 = J_3 = J_4 = 1$  corresponding to the “phase” where  $\gamma \geq \gamma_c(2, 2)$ . For the mode shown in this figure, we have  $W_x = 1, W_y = -1, \tilde{W}_x = 1, \tilde{W}_y = -1$ . There are 79 other configurations of the flux plaquettes and Wilson phases corresponding to the same eigenvalue as the first decay mode shown here.



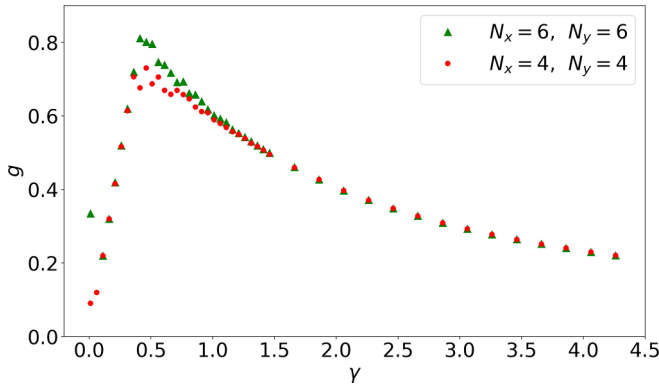


FIG. 10. Liouvillian gap,  $g$ , versus  $\gamma$  obtained over different runs of simulated annealing (all  $J_\delta = 1$ ) for  $4 \times 4$  and  $6 \times 6$  system sizes and even  $f$  parity. We used  $\alpha = 10$ ,  $T_0 = 100$  and a cycle consisted of 20 time steps. The number of runs was 10 for  $4 \times 4$  and 5 for  $6 \times 6$ . Some data points that are present at greater values of  $g$  are not shown in this cropped plot to focus on the features near the cusps in the plot.

different SA runs, and for different values of  $\gamma$ . We then use this set of field configurations as our pool to be tried for each value of  $\gamma$  in order to obtain an estimate of the minimum gap,  $g$ , by optimizing the relaxation rate gap with respect to allowed configurations. This yields the curves in Figs. 12–14. We do this only for even  $f$ -parity states, where the behavior corresponds to our analytical results from Sec. B at small and large  $\gamma$ . For the system sizes we have examined, the  $g(\gamma)$  curves all exhibit a linear behavior at small  $\gamma$ , crossing over to a  $1/\gamma$  behavior at large  $\gamma$ , as found by SK for their model [3]. While the gauge configurations obtained in this manner can vary from one  $\gamma$  value to the next, we found that the curves are largely unchanged by partitioning the  $\gamma$  line into three regimes, each of which is governed by a particular configuration of the gauge-invariant quantities [17] Note also the relatively small difference between the  $4 \times 4$  and  $6 \times 6$  results [18]. Among the configurations obtained in the different runs

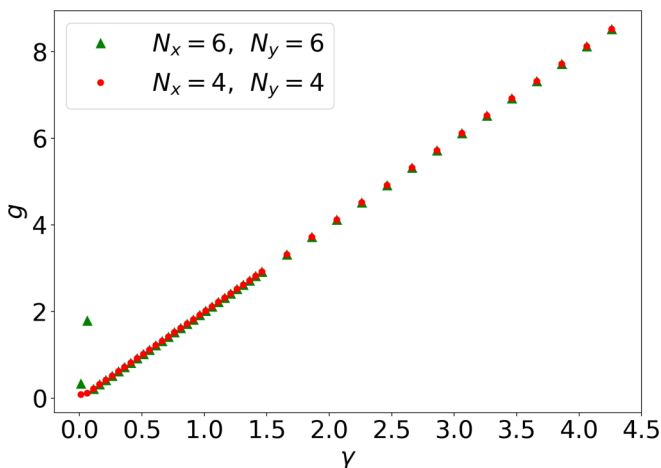


FIG. 11. Liouvillian gap,  $g$ , versus  $\gamma$  obtained over different runs of simulated annealing (all  $J_\delta = 1$ ) for  $4 \times 4$  and  $6 \times 6$  system sizes and odd  $f$  parity. We used  $\alpha = 10$ ,  $T_0 = 100$  and a cycle consisted of 20 time steps. The number of runs was 10 for  $4 \times 4$  and 5 for  $6 \times 6$ .

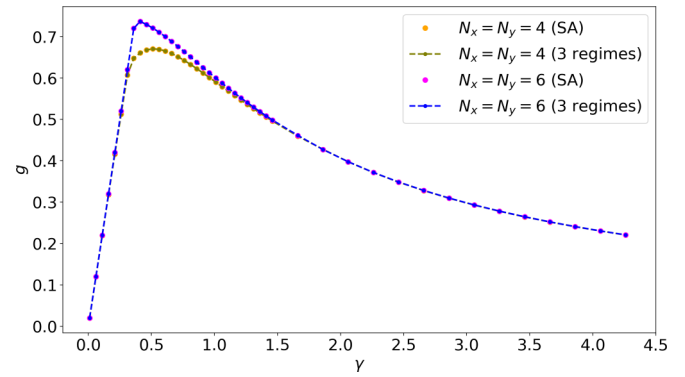


FIG. 12. Simulated annealing results for all  $J_\delta = 1$  and even  $f$  parity (see text for fuller description).

of simulated annealing, we tried to locate configurations that were closest to the predictions of the perturbative analysis in Appendix B. We used those modes to generate the corresponding behavior (i.e., the gap) at small and large  $\gamma$ . The results are shown in Fig. 15 and Fig. 16. These or some other degenerate modes could correspond to the eigenvalues obtained in the perturbative analysis.

SK found a sharp transition in the first decay modes between two regimes of dissipation strength, regardless of system size. (SK examined their model with open boundaries, but we have confirmed this result when periodic boundary conditions are applied to their model as well.) We cannot conclude whether or not this is the case for our model, but the intermediate regime we find could result from a failure of simulated annealing to reach the block of true first decay modes. We then try to investigate the gaps by fixing the number of vortices. This is addressed in Appendix E.

From simulated annealing, the optimal flux configurations for the lowest nonzero decay typically contain many defects. We list some of these configurations in the Appendix Sec. D below. For example, for the  $4 \times 4$  system with all  $J_\delta = 1$ , the optimal excited state we obtained had 11 defects relative to the fiducial NESS with all  $\mathbb{Z}_2$  data set to  $-1$ . However, since

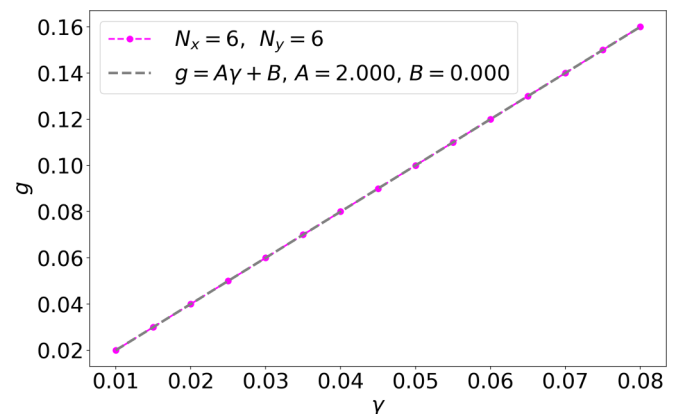


FIG. 13. Behavior at small  $\gamma$  for the largest system size we used in our calculations ( $6 \times 6$ ), with all  $J_\delta = 1$ . We obtained this curve by using the first decay modes we used to explain the small  $\gamma$  regime in Fig. 12.

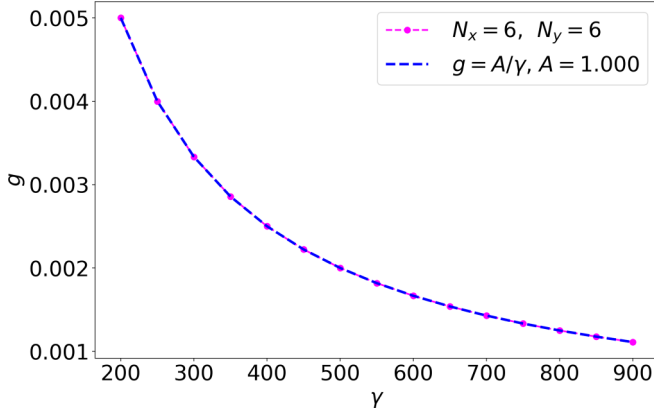


FIG. 14. Behavior at large  $\gamma$  for the largest system size we used in our calculations ( $6 \times 6$ ), with all  $J_\delta = 1$ . We obtained this curve by using the first decay modes we used to explain the large  $\gamma$  regime in Fig. 12.

we start the SA from a configuration of random  $\mathbb{Z}_2$  data, it may well be that a configuration with 11 defects with respect to a particular NESS might be described by fewer defects with respect to a different state in the  $2^{3N+1}$ -fold block of NESS. Our understanding of the minimal defect content of the degenerate excited states is very limited. An attempt to identify trends in this regard is shown in Appendix E where we study how the gap changes with number of vortices.

We try fitting the  $g(\gamma)$  curves to identify their behavior for small and large values of the dissipation strength  $\gamma$  (see Figs. 13 and 14). The shape of the  $g(\gamma)$  curves is similar to that found by Shibata and Katsura [3], rising linearly from zero at small  $\gamma$  and decaying as  $1/\gamma$  for large  $\gamma$ . In the Appendix B, we provide analytical support for these behaviors.

We also investigate the behavior of the gap for the case  $(J_1, J_2, J_3, J_4) = (3, 4, 1, 2)$ , which breaks certain discrete translation and rotation symmetries present in the model when

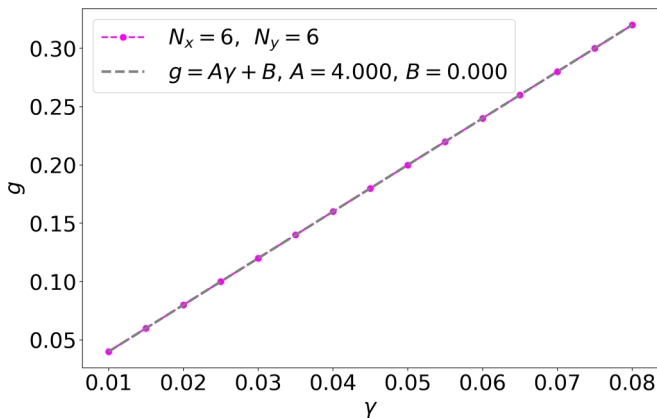


FIG. 15. Choosing a mode that behaves like  $g \approx 4\gamma$  at small  $\gamma$  for the largest system size we used in our calculations ( $6 \times 6$ ), with all  $J_\delta = 1$ . We depict the flux configuration corresponding to this mode by mentioning, relative to the NESS (in which all gauge-invariant  $\mathbb{Z}_2$  data is  $-1$ ), where the  $+1$  “defects” (i.e., gauge invariant quantities) exist:  $\Phi_{3,1}^+, \Phi_{5,1}^+, \Phi_{6,2}^-, \Phi_{1,3}^-, \Phi_{3,3}^-, \Phi_{4,2}^+, \Phi_{5,3}^-, \Phi_{3,3}^+, \Phi_{4,4}^-, \Phi_{6,4}^-, \Phi_{1,5}^-, \Phi_{3,5}^+, \Phi_{4,4}^+, \Phi_{5,5}^+, \Phi_{3,5}^-, \Phi_{1,1}^-, \Phi_{3,1}^-, \Phi_{6,6}^+, \Omega_{1,1}^+, \Omega_{5,3}^-, \Omega_{5,5}^-, \Omega_{1,1}^+, \Psi_{1,1}^+, \Psi_{1,1}^-, \Psi_{4,4}^+, \Psi_{6,4}^-, W_x$ , and  $W_y$ .

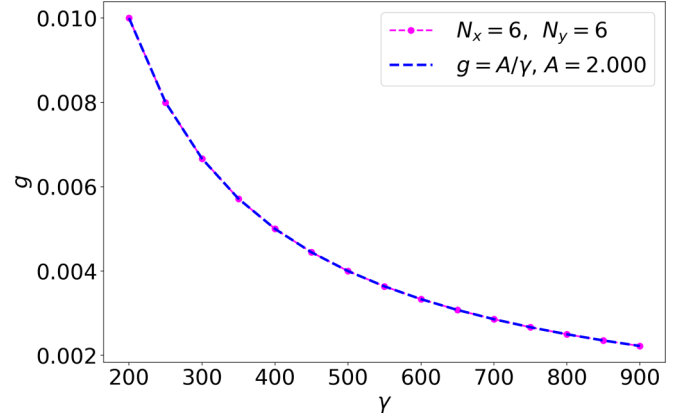


FIG. 16. Choosing a mode that behaves like  $g \approx 2/\gamma$  at large  $\gamma$  for the largest system size we used in our calculations ( $6 \times 6$ ), with all  $J_\delta = 1$ . We depict the flux configuration corresponding to this mode by mentioning, relative to the NESS (in which all gauge-invariant  $\mathbb{Z}_2$  data is  $-1$ ), where the  $+1$  “defects” (i.e., gauge invariant quantities) exist:  $\Phi_{1,1}^+, \Phi_{2,2}^-, \Phi_{3,1}^+, \Phi_{4,2}^-, \Phi_{6,2}^-, \Phi_{3,3}^-, \Phi_{4,2}^+, \Phi_{5,3}^-, \Phi_{1,3}^+, \Phi_{2,4}^-, \Phi_{3,3}^+, \Phi_{4,4}^+, \Phi_{5,3}^-, \Phi_{6,4}^+, \Phi_{4,4}^+, \Phi_{1,5}^-, \Phi_{2,6}^-, \Phi_{4,6}^-, \Phi_{1,1}^-, \Phi_{4,6}^+, \Phi_{5,1}^-, \Phi_{6,6}^+, \Omega_{6,4}^+, \Psi_{6,4}^-, W_x$ , and  $W_y$ .

all  $J_\delta$  are equal. The results are shown in Figs. 17 and 18 for a  $2 \times 2$  system. The study of this for larger system sizes and a comparison to the  $J_\delta = 1$  case is provided in Appendix E.

## V. CONCLUSIONS

In this paper we have described a two-dimensional square lattice model of interacting gamma matrix “spins” coupled to a dissipative environment. The density matrix evolution is described by the GKLS master equation  $\dot{\rho} = \mathcal{L}\rho$ , where  $\mathcal{L}$  is the Liouvillian, which in general has complex eigenvalues  $\Lambda_a$ . This description is equivalent to Schrödinger evolution under a non-Hermitian Hamiltonian  $\mathcal{W}$  on a square lattice bilayer, whose eigenvalues are  $E_a = -i\Lambda_a$ . Our model is inspired by, and a generalization of, the dissipative one-dimensional Pauli matrix spin model of Shibata and Katsura [3]. It is in the

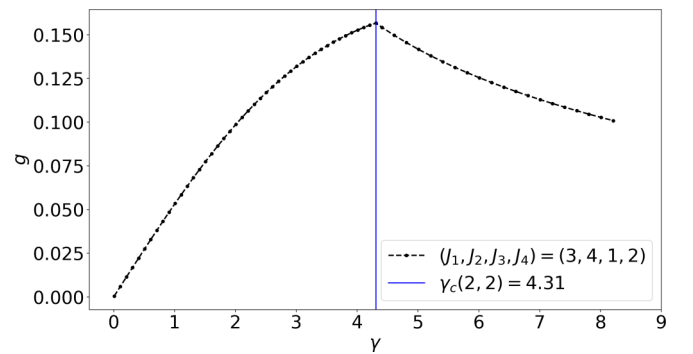


FIG. 17. Liouvillian gap  $g$  as a function of  $\gamma$  for our model with periodic boundary conditions for  $N_x = N_y = 2$  and  $(J_1, J_2, J_3, J_4) = (3, 4, 1, 2)$ , and with even  $f$  parity. There is a transition in the first decay modes at the cusp seen at  $\gamma = \gamma_c(2, 2)$ , depicted by the blue vertical line. We see a transition in the first decay modes. We have two first decay modes for  $\gamma < \gamma_c(2, 2)$  and eight first decay modes for  $\gamma \geq \gamma_c(2, 2)$ .

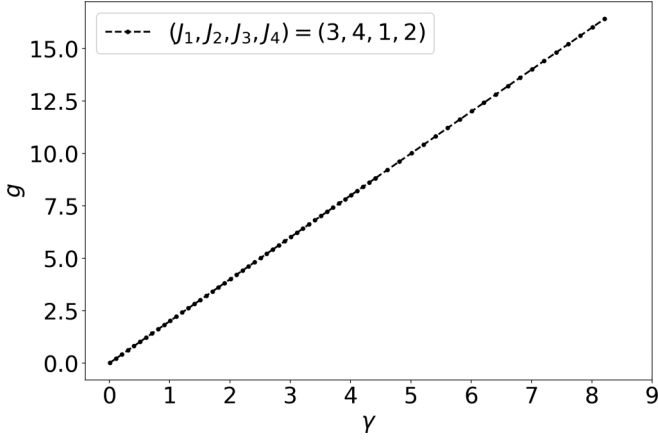


FIG. 18. Liouvillian gap  $g$  as a function of  $\gamma$  for our model with periodic boundary conditions for  $N_x = N_y = 2$  and  $(J_1, J_2, J_3, J_4) = (3, 4, 1, 2)$ , and with odd  $f$  parity. Unlike the even  $f$ -parity case, there is no cusp in the plot. We observe changes in the number of first decay modes at several values of  $\gamma$ .

“solvable” class of models exemplified by Kitaev’s celebrated honeycomb lattice model [5], equivalent to a single species of Majorana fermion hopping in a nondynamical  $\mathbb{Z}_2$  background gauge field. It is solvable in the sense that for any given configuration of the gauge-invariant plaquette fluxes and Wilson phases, the non-Hermitian Hamiltonian  $\mathcal{W}$  is quadratic and solvable by Prosen’s method [2]. However, there are exponentially many such configurations, and when the gauge field structure is not translationally invariant, the Hamiltonian must be diagonalized numerically. Furthermore, there is no analog of Lieb’s theorem [6] to assist us in identifying the longest lived decaying eigenmodes.

In the infinite time limit, the system approaches one of an exponentially large number of nonequilibrium steady states, with a spectrum  $\{-\text{Im} E_a\}$  of relaxation rates. The minimum relaxation rate  $g(\gamma)$  is typically achieved for different  $\mathbb{Z}_2$  flux configurations in the small and large  $\gamma$  limits, a feature also observed by Shibata and Katsura.

Other than in Fig. 19, we have not indicated in our plots the spectrum  $\{\text{Re} E_a\}$  of the real parts of the eigenvalues of

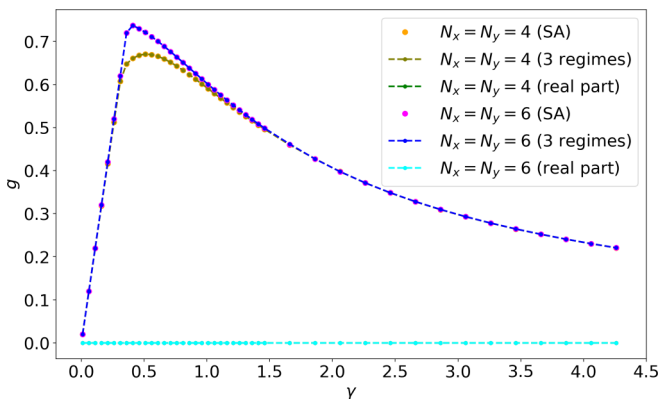


FIG. 19. Imaginary ( $g$ ) and real parts of the lowest decay modes as a function of  $\gamma$  for  $4 \times 4$  and  $6 \times 6$  lattices, with  $(J_1, J_2, J_3, J_4) = (1, 1, 1, 1)$ .  $\text{Re} E_a = 0$  for the case shown.

$\mathcal{W}$ . This is because in almost all cases studied we have found  $\text{Re} E_a = 0$  for the first decay mode [19]. When all  $J$ ’s are different, we find  $\text{Re} E_a = 0$  for the lowest decay modes, for all  $\gamma$  and all sizes.

Our model can further be generalized to other lattices. The Kitaev solvability of the SK model is associated with the fact that their model is equivalent to non-Hermitian Hamiltonian evolution on a two leg ladder, where each site lies at the confluence of three distinct classes of links. For the dimension  $k$  Clifford algebra, we have  $2k + 1$  gamma matrices of dimension  $2^k$ , and a Kitaev Hamiltonian (Hermitian or not) can be constructed on any lattice where each site lies at the confluence of  $(2k + 1)$  distinct classes of links [8]. Thus, for  $k = 2$ , our square lattice bilayer is fivefold coordinated. A corresponding model could thus be constructed on the kagome lattice, leading to a non-Hermitian Dirac matrix Hamiltonian  $\mathcal{W}$  on the kagome bilayer. (Further generalizations of this construction can result in multiple species of hopping and hybridizing Majoranas in the presence of a background non-dynamical gauge field, as in Refs. [7,14].) Thus, proceeding to  $k = 3$  with its seven  $8 \times 8$  gamma matrices, a corresponding model can be constructed on a cubic lattice (bipartite NaCl structure) with  $\Gamma_{\mathbf{R}}^{\delta} \Gamma_{\mathbf{R}+\delta}^{\delta}$  interactions on each class  $\delta$  link with  $\delta \in \{1, \dots, 6\}$  and Lindblad jump operators  $\sqrt{\gamma} \Gamma_{\mathbf{r}}^7$  at each site. Again, there will be an exponentially large block of NESS density matrices owing to the conserved plaquette fluxes.

*Note added.* Recently, an analysis of two largely equivalent models appeared on the arXiv [10,11].

## ACKNOWLEDGMENTS

We gratefully acknowledge conversations with T. Grover and J. McGreevy. We thank D. Chowdhury for alerting us to Ref. [11]. This research was funded in part by General Campus Research Award RG104654 from the UC San Diego Academic Senate. D.P.A. acknowledges the hospitality of the Aspen Center of Physics where some of this work was completed.

## APPENDIX A: FERMION PARITY

Equation (34) describes the condition on the parity of the  $c$ -fermions for a state to belong to the physical subspace. The non-Hermitian Hamiltonian in Eq. (20) may be written as

$$\mathcal{W} = \frac{i}{4} \theta_i A_{ij} \theta_j + W_0, \quad (\text{A1})$$

where  $A$  is a  $d \times d$  complex antisymmetric, here with  $d = 2N$ , whose elements depend on the static  $\mathbb{Z}_2$  gauge configuration  $\mathcal{G} \equiv \{u_{\mathbf{R}}^{\alpha}, \tilde{u}_{\mathbf{R}}^{\alpha}, u_{\mathbf{r}}^5\}$ , and where  $\theta_{j+N}^0 = \tilde{\theta}_j^0$ , and  $W_0 = -2i\gamma N_c$  is a constant. We follow the method of Prosen [2] to diagonalize the matrix  $A$ .

To diagonalize the matrix  $A$  we use the method of Prosen [2]. We define  $V$  as the matrix of right (column) eigenvectors of  $A$ . Assuming there are no zero eigenvalues, which means  $d$  is even, we may write  $A = V \Lambda V^T$  with

$$\Lambda = \begin{pmatrix} 0 & \lambda_1 \\ -\lambda_1 & 0 \end{pmatrix} \oplus \dots \oplus \begin{pmatrix} 0 & \lambda_n \\ -\lambda_n & 0 \end{pmatrix} \quad (\text{A2})$$

and

$$X \equiv V^\top V = \begin{pmatrix} 0 & 1 \\ 1 & 0 \end{pmatrix} \oplus \dots \oplus \begin{pmatrix} 0 & 1 \\ 1 & 0 \end{pmatrix}, \quad (\text{A3})$$

where  $n = d/2$ . The  $\{\pm\lambda_a\}$ , with  $a \in \{1, \dots, n\}$ , are the eigenvalues of  $A$ . When there are zero eigenvalues (there is always at least one zero eigenvalue when  $d$  is odd), then  $2n < d$  and the above expression for  $\Lambda$  is appended by taking its direct sum with a  $d - 2n$ -dimensional block of zeros, while  $X$  is appended with a  $d - 2n$  identity matrix. Here we take  $d = 2N$  even and for simplicity assume no zero eigenvalues. We may then take  $\text{Re } \lambda_N \geq \text{Re } \lambda_{n-1} \geq \dots \geq \text{Re } \lambda_1 > 0$ .

Defining the operators  $\zeta_a \equiv \theta_i V_{ia}$ , one has  $\{\zeta_a, \zeta_b\} = 2X_{ab}$ . One can go on to define

$$f_p^\ddagger \equiv \frac{1}{\sqrt{2}} \zeta_{2p-1}, \quad f_p \equiv \frac{1}{\sqrt{2}} \zeta_{2p}, \quad (\text{A4})$$

with  $p \in \{1, \dots, N\}$ . These operators satisfy the anticommutation relations of complex fermions,

$$\{f_p, f_q\} = \{f_p^\ddagger, f_q^\ddagger\} = 0, \quad \{f_p, f_q^\ddagger\} = \delta_{pq}, \quad (\text{A5})$$

but with the important distinction that  $f_p^\ddagger \neq f_p^\dagger$ , which is due to the fact that  $\zeta_a^\dagger = \theta_i V_{ia}^* \neq \zeta_a$ .

$$\mathcal{W} = i \sum_{p=1}^n \lambda_p \left( f_p^\ddagger f_p - \frac{1}{2} \right) + W_0. \quad (\text{A6})$$

$$\mathcal{W} = \frac{i}{4} (\mathbf{c}^\dagger \quad \mathbf{c}) \begin{pmatrix} A^{bb} + A^{tt} + iA^{bt} - iA^{tb} & A^{bb} - A^{tt} - iA^{bt} - iA^{tb} \\ A^{bb} - A^{tt} + iA^{bt} + iA^{tb} & A^{bb} + A^{tt} - iA^{bt} + iA^{tb} \end{pmatrix} \begin{pmatrix} \mathbf{c} \\ \mathbf{c}^\dagger \end{pmatrix} + W_0, \quad (\text{A10})$$

The condition that there are no pairing terms  $c_r^\dagger c_s^\dagger$  or  $c_r c_s$  is then  $A^{tt} = A^{bb}$  and  $A^{tb} = -A^{bt}$ . These two conditions guarantee that the upper right and lower left blocks of the above  $2N \times 2N$  matrix  $A$  are all zeros. Under these circumstances, we have

$$\begin{aligned} \mathcal{W} &= \frac{1}{2} (\mathbf{c}^\dagger \quad \mathbf{c}) \begin{pmatrix} iA^{bb} - A^{bt} & 0 \\ 0 & iA^{bb} + A^{bt} \end{pmatrix} \begin{pmatrix} \mathbf{c} \\ \mathbf{c}^\dagger \end{pmatrix} + W_0 \\ &= c_r^\dagger M_{rs} c_s + W_0 + \Delta W_0, \end{aligned} \quad (\text{A11})$$

where

$$M_{rs} = -\frac{1}{2} (A_{rs}^{bt} + A_{sr}^{bt}) + iA_{rs}^{bb}, \quad \Delta W_0 = \frac{1}{2} \text{Tr} A^{bt}. \quad (\text{A12})$$

Note that, in general,  $M \in \text{GL}(n, \mathbb{C})$  has both symmetric and antisymmetric components, i.e., it is a general complex  $N \times N$  matrix.

Assuming there are no Jordan blocks, the matrix  $M$  may then be decomposed in terms of its right and left eigenvectors as

$$M_{rs} = \sum_{p=1}^n \varepsilon_p R_r^p L_s^p, \quad (\text{A13})$$

or in bracket notation  $M = \sum_p \varepsilon_p |R^p\rangle \langle L^p|$ . With no Jordan blocks, the eigenvectors span, in which case

$$\sum_{p=1}^n R_r^p L_s^p = \delta_{rs}, \quad \sum_{r=1}^n R_r^p L_r^\beta = \delta^{p\beta}, \quad (\text{A14})$$

The  $f$  parity of a state is defined to be the parity of the occupation number sum  $\sum_{p=1}^N f_p^\ddagger f_p$  in that state.

We can break the matrix  $A$  into four  $N \times N$  blocks with  $b$  (bottom layer) and superindices  $t$  (top layer), viz.,

$$\mathcal{W} - W_0 = \frac{i}{4} \sum_{r,s=1}^N \begin{pmatrix} \theta_r^0 & \tilde{\theta}_r^0 \\ A_{rs}^{bb} & A_{rs}^{bt} \\ A_{rs}^{tb} & A_{rs}^{tt} \end{pmatrix} \begin{pmatrix} \theta_s^0 \\ \tilde{\theta}_s^0 \end{pmatrix}, \quad (\text{A7})$$

where

$$\begin{aligned} A_{rs}^{bb} &= A_{r,s}, & A_{rs}^{bt} &= A_{r,s+N}, & A_{rs}^{tb} &= A_{r+N,s}, \\ A_{rs}^{tt} &= A_{r+N,s+N}. \end{aligned} \quad (\text{A8})$$

Antisymmetry of  $A$  then implies

$$A_{rs}^{tt} = -A_{sr}^{tt}, \quad A_{rs}^{bb} = -A_{sr}^{bb}, \quad A_{rs}^{tb} = -A_{sr}^{bt}, \quad (\text{A9})$$

i.e.,  $(A^{bb})^\top = -A^{bb}$ ,  $(A^{tt})^\top = -A^{tt}$ , and  $(A^{tb})^\top = -A^{bt}$ , all in  $\text{GL}(N, \mathbb{C})$ . From Eq. (27), one then has

which are the completeness and orthogonality relations, respectively. We define the operators

$$g_p = \langle L^p | c \rangle = \sum_{r=1}^n L_r^p c_r, \quad g_p^\ddagger = \langle c^\dagger | R^p \rangle = \sum_{r=1}^n R_r^p c_r^\dagger. \quad (\text{A15})$$

We then have  $\{g_p, g_q^\ddagger\} = \delta_{pq}$ . We then have

$$\mathcal{W} = \sum_{p=1}^n \varepsilon_p g_p^\ddagger g_p + W_0 + \Delta W_0. \quad (\text{A16})$$

Furthermore,

$$\sum_{p=1}^n g_p^\ddagger g_p = \sum_{p=1}^n \langle c^\dagger | R^p \rangle \langle L^p | c \rangle = \langle c^\dagger | c \rangle = \sum_{r=1}^n c_r^\dagger c_r \quad (\text{A17})$$

and  $\widehat{N}_g = \widehat{N}_c$ . Note that the diagonalized  $\mathcal{W}$  in Eq. (A6) is given by

$$\mathcal{W} = \sum_{p=1}^n i\lambda_p f_p^\ddagger f_p - \frac{1}{2} \sum_{p=1}^n i\lambda_p + W_0. \quad (\text{A18})$$

Thus in the absence of pairing terms we apparently may identify

$$g_p \equiv f_p, \quad g_p^\ddagger \equiv f_p^\ddagger, \quad \varepsilon_p \equiv i\lambda_p, \quad \Delta W_0 = -\frac{1}{2} \sum_{p=1}^n \varepsilon_p. \quad (\text{A19})$$



From Eq. (18), the local constraint at each site  $r$  in each layer is

$$\theta_r^0 \theta_r^1 \theta_r^2 \theta_r^3 \theta_r^4 \theta_r^5 = i, \quad \tilde{\theta}_r^0 \tilde{\theta}_r^1 \tilde{\theta}_r^2 \tilde{\theta}_r^3 \tilde{\theta}_r^4 \tilde{\theta}_r^5 = i, \quad (\text{A20})$$

Now take the product over all sites  $r$  in each layer. One obtains the relation

$$\prod_R \Phi_R^+ \cdot \prod_R \tilde{\Phi}_R^+ \cdot \prod_r u_r^5 \cdot \prod_r i\theta_r^0 \tilde{\theta}_r^0 = 1, \quad (\text{A21})$$

where the products of  $\Phi_R^+$  and  $\tilde{\Phi}_R^+$  in each layer are over half the square plaquettes, i.e., the ‘‘white chessboard squares’’ only. In the language of Ref. [7], which describes a (Hermitian) square lattice Dirac matrix spin model, the  $\theta_r^0$  and  $\theta_r^5$  Majoranas combine to yield a complex fermion at each site  $r$ . The fermion parity is then fixed by the gauge-invariant plaquette fluxes due to the projection onto the physical sector. In our model, there are two layers, and the  $\theta_r^5$  and  $\tilde{\theta}_r^5$  Majoranas combine to form the gauge fields  $u_r^5$  on each link connecting the planes, while the  $\theta_r^0$  and  $\tilde{\theta}_r^0$  fermions combine to form the complex  $(c_r, c_r^\dagger)$  fermions as described in Eq. (28). Thus the constraint as expressed in Eq. (A21) involves the gauge-invariant fluxes  $\{\Phi_R^+, \tilde{\Phi}_R^+\}$ , the fermion occupations  $i\theta_r^0 \tilde{\theta}_r^0 = 2c_r^\dagger c_r - 1$ , and the gauge-dependent quantities  $\{u_r^5\}$ . Apparently, then, there is no way to identify the physical fermion parity based on gauge-invariant data alone. The problem is particularly acute when there are pairing terms in  $\mathcal{W}$ . Nevertheless, as described in Sec. IV above, we find it useful to classify the eigenstates of  $\mathcal{W}$  by their  $f$  parity, with  $N_f \equiv \sum_p f_p^\dagger f_p$  even (typically 0 or 2), or  $N_f$  odd (typically 1).

## APPENDIX B: PERTURBATION THEORY FOR LARGE AND SMALL VALUES OF $\gamma$

Can *et al.* [20] considered a model of a random Hermitian Hamiltonian  $H$  in the presence of a single Hermitian jump operator  $\sqrt{\gamma}L$ , with both  $H$  and  $L$  random and chosen from the Gaussian unitary ensemble. They showed how the spectrum of relaxation times could be computed perturbatively in the small and large  $\gamma$  limits, by perturbing in the dissipator  $\mathcal{L}_D = \frac{1}{2}\gamma[L, [\bullet, L]]$  or in the nondissipative Liouvillian  $\mathcal{L}_H = -i[H, \bullet]$ , respectively. Thus, at small  $\gamma$ , the smallest nonzero relaxation rate  $\tau^{-1}$  is proportional to  $\gamma$ , while at large  $\gamma$  it is proportional to  $\gamma^{-1}$ . In this Appendix we perform a related analysis for our model.

### 1. $\gamma \ll 1$

For  $\gamma \ll 1$  we write the GKLS equation as a classical master equation for the projectors  $P_\alpha = |\alpha\rangle\langle\alpha|$ , where  $\alpha$  is an eigenstate of the Hamiltonian  $H$  [20]. This classical master equation is written

$$\frac{dP_\alpha}{dt} = \gamma \mathcal{M}_{\alpha\beta} P_\beta, \quad (\text{B1})$$

with

$$\mathcal{M}_{\alpha\beta} = \sum_r (|\langle\alpha|\Gamma_r^5|\beta\rangle|^2 - N\delta_{\alpha\beta}). \quad (\text{B2})$$

Clearly this analysis will lead in this limit to real eigenvalues proportional to  $\gamma$ . What is the coefficient for the smallest such eigenvalue?

To analyze this, we start with our Hamiltonian,

$$H = i \sum_{R \in A} \sum_{\delta=1}^4 J_\delta u_R^\delta \theta_R^0 \theta_{R+\delta}^0 \equiv \frac{i}{2} \sum_{r,r'} J_{r,r'} \theta_r^0 \theta_{r'}^0, \quad (\text{B3})$$

where  $J_{r,r'}$  is a real antisymmetric matrix with  $J_{R,R+\delta} = J^\delta u_R^\delta$ . The  $\theta_r^5$  Majoranas are cyclic in  $H$  and lead to an exponential degeneracy  $\sim 2^{N_c}$  for each energy level. Including the  $N-1$  plaquette fluxes and the two Wilson phases, and accounting for the constraint

$$\prod_r i\theta_r^0 \theta_r^1 \theta_r^2 \theta_r^3 \theta_r^4 \theta_r^5 = 1, \quad (\text{B4})$$

which constrains the combined parity of the  $a=0$  and  $a=5$  species fermions given the gauge fields  $u_{rr'}$ , we have a total of  $4^N$  projectors:  $2^{N+1}$  from plaquette fluxes and Wilson phases (see Fig. 5), and  $2^{N-1}$  for the parity-constrained  $a=0, 5$  fermions. This is a subset of the  $16^N$  (unnormalized) density matrices.

Every real antisymmetric matrix can be diagonalized by an orthogonal transformation. For each gauge field configuration, the corresponding real antisymmetric matrix  $J_{rr'}$  is brought to block diagonal form by a real orthogonal matrix  $Q_{r,s}$ , such that

$$Q^T J Q = \begin{pmatrix} 0 & \varepsilon_1 \\ -\varepsilon_1 & 0 \end{pmatrix} \oplus \dots \oplus \begin{pmatrix} 0 & \varepsilon_{N_c} \\ -\varepsilon_{N_c} & 0 \end{pmatrix}, \quad (\text{B5})$$

where  $\{\varepsilon_s\}$  are the singular values of  $J$  [21]. We define a new set of Majoranas  $\xi_s = \theta_r^0 Q_{r,s}$ , and we may associate each  $s$  with a site on the  $N_x \times N_y$  square lattice, exactly as is the case for the  $r$  sites. Thus, the  $s$  values are divided into **A** and **B** sublattices, and writing  $S \in \mathbf{A}$  we have  $S + \hat{x} \in \mathbf{B}$ . Each of the  $2 \times 2$  blocks in Eq. (B5) is then associated with  $s = S$  and  $s' = S + \hat{x}$ , for some  $S$ . We now define

$$c_S = \frac{1}{2}(\xi_S - i\xi_{S+\hat{x}}), \quad c_S^\dagger = \frac{1}{2}(\xi_S + i\xi_{S+\hat{x}}), \\ d_R = \frac{1}{2}(\theta_R^5 - i\theta_{R+\hat{x}}^5), \quad d_R^\dagger = \frac{1}{2}(\theta_R^5 + i\theta_{R+\hat{x}}^5), \quad (\text{B6})$$

which entail

$$\xi_S = c_S^\dagger + c_S, \quad \xi_{S+\hat{x}} = i(c_S^\dagger - c_S), \\ \theta_R^5 = d_R^\dagger + d_R, \quad \theta_{R+\hat{x}}^5 = i(d_R^\dagger - d_R). \quad (\text{B7})$$

The Hamiltonian is then  $H = \sum_S \varepsilon_S (2c_S^\dagger c_S - 1)$ . We may now write

$$\Gamma_R^5 = \sum_S \{i Q_{S,R}^{AA} (c_S^\dagger + c_S)(d_R^\dagger + d_R) \\ + Q_{S,R}^{BA} (c_S - c_S^\dagger)(d_R^\dagger + d_R)\} \\ \Gamma_{R+\hat{x}}^5 = \sum_S \{Q_{S,R}^{AB} (c_S^\dagger + c_S)(d_R - d_R^\dagger) \\ - i Q_{S,R}^{BB} (c_S - c_S^\dagger)(d_R - d_R^\dagger)\}, \quad (\text{B8})$$

where

$$\begin{aligned} Q_{S,R}^{AA} &= Q_{S,R}, & Q_{S,R}^{AB} &= Q_{S,R+\hat{x}}, & Q_{S,R}^{BA} &= Q_{S+\hat{x},R}, \\ Q_{S,R}^{BB} &= Q_{S+\hat{x},R+\hat{x}}. \end{aligned} \quad (\text{B9})$$

Now consider the matrix elements  $\langle \mathbf{m}, \mathbf{n} | \Gamma_{\mathbf{R}}^5 | \mathbf{m}', \mathbf{n}' \rangle$  and  $\langle \mathbf{m}, \mathbf{n} | \Gamma_{\mathbf{R}+\hat{x}}^5 | \mathbf{m}', \mathbf{n}' \rangle$ , where

$$|\mathbf{m}, \mathbf{n}\rangle \equiv \prod_S (c_S^\dagger)^{m_S} \prod_{\mathbf{R}} (d_{\mathbf{R}}^\dagger)^{n_{\mathbf{R}}} |0\rangle, \quad (\text{B10})$$

where  $|0\rangle$  is the vacuum for  $c$  and  $d$  fermions. Then

$$\begin{aligned} &\sum_{\mathbf{r}} |\langle \mathbf{m}, \mathbf{n} | \Gamma_{\mathbf{r}}^5 | \mathbf{m}', \mathbf{n}' \rangle|^2 \\ &= \sum_{\mathbf{R}_1} \sum_{S_1} [ (Q_{S_1, \mathbf{R}_1}^{AA})^2 + (Q_{S_1, \mathbf{R}_1}^{AB})^2 + (Q_{S_1, \mathbf{R}_1}^{BA})^2 + (Q_{S_1, \mathbf{R}_1}^{BB})^2 ] \\ &\quad \times \tilde{\delta}_{\mathbf{m}, \mathbf{m}', S_1} \tilde{\delta}_{\mathbf{n}, \mathbf{n}', \mathbf{R}_1}, \end{aligned} \quad (\text{B11})$$

where we have defined the symbol

$$\tilde{\delta}_{\mathbf{m}, \mathbf{m}', S_1} = \delta_{m'_{S_1}, 1-m_{S_1}} \times \prod_{S \neq S_1} \delta_{m'_S, m_S}. \quad (\text{B12})$$

In other words,  $\tilde{\delta}_{\mathbf{m}, \mathbf{m}', S_1} = 1$  when  $m'_S = m_S$  for all  $S$  other than  $S_1$ , where the two occupations are complementary.

When the gauge fields have the periodicity of the lattice, i.e., when  $u_{\mathbf{R}}^\delta = u_{\mathbf{R}'}^\delta$  for all  $\mathbf{R}$  and  $\mathbf{R}'$ , translational invariance allows us to simplify Eq. (B11), in which case

$$\mathcal{M}_{\mathbf{m}, \mathbf{m}', S_1} = \frac{4}{N} \delta_{d(\mathbf{m}, \mathbf{m}'), 1} \delta_{d(\mathbf{n}, \mathbf{n}'), 1} - N \delta_{\mathbf{m}, \mathbf{m}'} \delta_{\mathbf{n}, \mathbf{n}'}, \quad (\text{B13})$$

where  $d(\mathbf{m}, \mathbf{m}')$  is the number of locations where the occupation  $m_S$  differs from  $m'_S$ . The eigenvalues of  $\mathcal{M}$  are then given by

$$\Lambda(\boldsymbol{\sigma}, \boldsymbol{\mu}) = \frac{4}{N} (\sigma_1 + \dots + \sigma_{N_c}) (\mu_1 + \dots + \mu_{N_c}) - N, \quad (\text{B14})$$

where each  $\sigma_S$  and  $\mu_{\mathbf{R}}$  are either  $+1$  or  $-1$ . When all  $\sigma_S$  and  $\mu_{\mathbf{R}}$  are  $+1$  or all are  $-1$ , the eigenvalue is zero, corresponding to a NESS. When one of the  $\sigma$  or  $\mu$  values has a reversed sign, we obtain  $\Lambda = -4$ , corresponding to a Liouvillian eigenvalue of  $-4\gamma$ . Numerically, we find that the slope of the smallest nonzero decay rate  $-\text{Re } \Lambda(\boldsymbol{\sigma}, \boldsymbol{\mu})$  is 2 rather than 4. It may be that for sectors of  $\mathcal{M}$  corresponding to nontranslationally invariant flux configurations, where the  $Q$  matrices do not reflect such a symmetry, that the coefficient for the lowest decay rate is smaller, but we do not understand how to arrive at a slope of 1. Another possibility we have not explored is the dynamics of a restricted class of coherences  $|\alpha\rangle\langle\beta|$ , where  $|\alpha\rangle = |\mathbf{m}, \mathbf{n}_1\rangle$  and  $|\beta\rangle = |\mathbf{m}, \mathbf{n}_2\rangle$ . There are  $2^{5N/2}$  such coherences, all of which commute with  $H$ , arranged into  $2^N$  blocks of size  $2^{3N/2}$ . The generalization of the matrix  $\mathcal{M}$  in each block is then

$$\begin{aligned} &\mathcal{M}_{\mathbf{m}, \mathbf{n}_1, \mathbf{n}_2, \mathbf{M}, N_1, N_2} \\ &= \sum_{\mathbf{r}} (\langle \mathbf{M}, N_1 | \Gamma_{\mathbf{r}}^5 | \mathbf{m}, \mathbf{n}_1 \rangle \langle \mathbf{m}, \mathbf{n}_2 | \Gamma_{\mathbf{r}}^5 | \mathbf{M}, N_2 \rangle \\ &\quad - N \delta_{\mathbf{M}, \mathbf{m}} \delta_{\mathbf{M}_1, \mathbf{n}_1} \delta_{\mathbf{M}_2, \mathbf{n}_2} ). \end{aligned} \quad (\text{B15})$$

While the the matrix element products

$$\langle N_1 | d_{\mathbf{R}}^\dagger \pm d_{\mathbf{R}} | \mathbf{n}_1 \rangle \langle \mathbf{n}_2 | d_{\mathbf{R}}^\dagger \pm d_{\mathbf{R}} | N_2 \rangle \quad (\text{B16})$$

are nonzero only if  $N_1$  and  $\mathbf{n}_1$  have complementary occupancies in the same location  $\mathbf{R}$  as do  $N_2$  and  $\mathbf{n}_2$ , the presence of occupation number dependent sign factors complicates the analysis.

## 2. $\gamma \gg 1$

We start with the Dirac matrices,

$$\begin{aligned} \Gamma^1 &= X \otimes 1 = \begin{pmatrix} 0 & 0 & 1 & 0 \\ 0 & 0 & 0 & 1 \\ 1 & 0 & 0 & 0 \\ 0 & 1 & 0 & 0 \end{pmatrix} \\ \Gamma^2 &= Y \otimes 1 = \begin{pmatrix} 0 & 0 & -i & 0 \\ 0 & 0 & 0 & -i \\ i & 0 & 0 & 0 \\ 0 & i & 0 & 0 \end{pmatrix} \\ \Gamma^3 &= Z \otimes X = \begin{pmatrix} 0 & 1 & 0 & 0 \\ 1 & 0 & 0 & 0 \\ 0 & 0 & 0 & -1 \\ 0 & 0 & -1 & 0 \end{pmatrix} \\ \Gamma^4 &= Z \otimes Y = \begin{pmatrix} 0 & -i & 0 & 0 \\ i & 0 & 0 & 0 \\ 0 & 0 & 0 & i \\ 0 & 0 & -i & 0 \end{pmatrix} \\ \Gamma^5 &= Z \otimes Z = \begin{pmatrix} 1 & 0 & 0 & 0 \\ 0 & -1 & 0 & 0 \\ 0 & 0 & -1 & 0 \\ 0 & 0 & 0 & 1 \end{pmatrix}. \end{aligned} \quad (\text{B17})$$

We label the eigenstates of  $\Gamma^5$  by an index  $\mu \in \{1, 2, 3, 4\}$ , with eigenvectors  $\psi_i^{(\mu)} = \delta_{i, \mu}$  and with eigenvalues  $\zeta_\mu = \{1, -1, -1, 1\}$ , respectively. Since  $\mathcal{L}_D \varrho = \gamma \sum_{\mathbf{r}} (\Gamma_{\mathbf{r}}^5 \varrho \Gamma_{\mathbf{r}}^5 - \varrho)$ , any operator  $|\boldsymbol{\mu}\rangle\langle\mathbf{v}|$  is annihilated by  $\mathcal{L}_D$  provided it is an eigenoperator under the action of  $\Gamma_{\mathbf{r}}^5$  from either the left or the right, at every site  $\mathbf{r}$ . There are  $8^N$  such operators, since we can freely choose each of the  $\mu_{\mathbf{r}}$  so long as  $v_{\mathbf{r}} = \mu_{\mathbf{r}}$  or  $v_{\mathbf{r}} = 5 - \mu_{\mathbf{r}}$ . In general, the eigenoperators of  $\mathcal{L}_D$  are arranged into sectors  $\Upsilon_k$ , where  $|\boldsymbol{\mu}\rangle\langle\mathbf{v}| \in \Upsilon_k$  provided  $\zeta_{\mu_{\mathbf{r}}} \neq \zeta_{v_{\mathbf{r}}}$  at  $k$  locations  $\mathbf{r}$ . The eigenvalue under  $\mathcal{L}_D$  for any operator in sector  $\Upsilon_k$  is then  $-2k\gamma$ .

We label the  $8^N$  operators in the  $\Upsilon_0$  sector as  $A_p = |\boldsymbol{\mu}\rangle\langle\mathbf{v}|$ , with  $p_{\mathbf{r}} = \mu_{\mathbf{r}}$  if  $v_{\mathbf{r}} = \mu_{\mathbf{r}}$  and  $p_{\mathbf{r}} = \mu_{\mathbf{r}} + 4$  if  $v_{\mathbf{r}} = 5 - \mu_{\mathbf{r}}$  at each site  $\mathbf{r}$ . We also define the  $2N \times 8^N$  operators

$$B_p^l = i |\boldsymbol{\mu}\rangle\langle\mathbf{v}| H_l - i H_l |\boldsymbol{\mu}\rangle\langle\mathbf{v}|, \quad (\text{B18})$$

where  $l$  denotes one of the  $2N$  links  $(\mathbf{R}, \mathbf{R} + \boldsymbol{\delta})$  and where  $H_l = J_\delta \Gamma_{\mathbf{R}}^\delta \Gamma_{\mathbf{R}+\boldsymbol{\delta}}^\delta$ . For simplicity we shall assume  $J_\delta = 1$  for each of the four types of links, although our method described below can easily be applied to the more general case. Since each of the matrices  $\Gamma^{1,2,3,4}$  anticommutes with  $\Gamma^5$ , its application reverses the  $\Gamma^5$  eigenvalue, and thus  $B_p^l \in \Upsilon_2$  for all  $p$

and links  $l$ . We then have

$$\mathcal{L}_H A_p = \sum_l B_p^l. \quad (\text{B19})$$

We wish to analyze the Liouvillian  $\mathcal{L} = \mathcal{L}_H + \mathcal{L}_D$  when restricted to the subspace  $\Upsilon_0 \cup \Upsilon'_2$ , where  $\Upsilon'_2 \subset \Upsilon_2$  includes operators  $|\mu\rangle\langle\nu|$  where there are differences in the  $\Gamma^5$  eigenvalues of the bra and ket states at two sites from the same link. In other words, we restrict the action of  $\mathcal{L}$  to the subspace of operators spanned by the  $A_p$  and the  $B_p^l$ . The total dimension

of this operator space is then  $(2N + 1) \cdot 8^N$ , since there are  $2N$  values of  $l$ .

We now need to evaluate  $\mathcal{L}_H B_p^l$ . We have

$$\mathcal{L}_H B_p^l = 2A_p^l - 2A_p + \dots, \quad (\text{B20})$$

where  $A_p^l \equiv H_l |\mu\rangle\langle\nu| H_l$ , which also this lives in sector  $\Upsilon_0$  provided  $|\mu\rangle\langle\nu| \in \Upsilon_0$ . The remaining terms include operators in other sectors  $\Upsilon_{k>2}$  and operators in  $\Upsilon_2$  where the differences in the  $\Gamma_r^5$  eigenvalues of the bra and ket states are at two sites not connected by a link, thus requiring two applications of  $\mathcal{L}_H$  to reach from  $\Upsilon_0$ . In this basis, the matrix form of the projected Liouvillian  $\tilde{\mathcal{L}}$  is

$$\tilde{\mathcal{L}} = \begin{pmatrix} \mathbb{0} & -2R_1 & -2R_2 & \dots & -2R_M \\ \mathbb{1} & -4\gamma\mathbb{1} & \mathbb{0} & - & \mathbb{0} \\ \mathbb{1} & \mathbb{0} & -4\gamma\mathbb{1} & - & \mathbb{0} \\ \vdots & - & - & \ddots & \vdots \\ \mathbb{1} & \mathbb{0} & \dots & & -4\gamma\mathbb{1} \end{pmatrix} \Rightarrow \omega - \tilde{\mathcal{L}} = \begin{pmatrix} \omega\mathbb{1} & 2R_1 & 2R_2 & \dots & 2R_M \\ -\mathbb{1} & (\omega + 4\gamma)\mathbb{1} & \mathbb{0} & & \mathbb{0} \\ -\mathbb{1} & \mathbb{0} & (\omega + 4\gamma)\mathbb{1} & & \mathbb{0} \\ \vdots & - & - & \ddots & \vdots \\ -\mathbb{1} & \mathbb{0} & \dots & & (\omega + 4\gamma)\mathbb{1} \end{pmatrix}, \quad (\text{B21})$$

where  $M = 2N$  is the number of links in the square lattice (with periodic boundary conditions) and  $\{R_1, \dots, R_M\}$  are  $8N \times 8N$  matrices. We can now perform row and column reduction on the matrix  $\omega - \tilde{\mathcal{L}}$  to obtain

$$\omega - \tilde{\mathcal{L}} \mapsto \begin{bmatrix} \omega & 2S_M & 2S_{M-1} & \dots & - & 2S_1 \\ -\mathbb{1} & (\omega + 4\gamma)\mathbb{1} & \mathbb{0} & & - & \mathbb{0} \\ \mathbb{0} & \mathbb{0} & (\omega + 4\gamma)\mathbb{1} & & & \mathbb{0} \\ \mathbb{0} & \mathbb{0} & \mathbb{0} & & & \mathbb{0} \\ \vdots & - & - & \ddots & - & \vdots \\ - & - & - & & (\omega + 4\gamma)\mathbb{1} & \mathbb{0} \\ \mathbb{0} & \dots & - & \mathbb{0} & & (\omega + 4\gamma)\mathbb{1} \end{bmatrix}, \quad (\text{B22})$$

where  $S_k = \sum_{l=1}^k R_l$ , and the characteristic polynomial is

$$P(\omega) = (\omega + 4\gamma)^{(M-1)D} \det(\omega^2 + 4\gamma\omega + 2S), \quad (\text{B23})$$

where  $D = 8^N$  and where we define  $S \equiv S_M$ . Thus there are  $(M - 1)D$  degenerate eigenvalues with  $\omega = -4\gamma$  and  $2D$  eigenvalues,

$$\omega_{j,\pm} = -2\gamma \pm \sqrt{4\gamma^2 - 2s_j}, \quad (\text{B24})$$

where  $\{s_j\}$  are the  $D$  eigenvalues of the matrix  $S$ . In the limit  $\gamma \gg s_j$  we then have  $\omega_{-,j} = -s_j/2\gamma + \mathcal{O}(\gamma^{-2})$ . Regarding the row and column reduction of  $\omega - \tilde{\mathcal{L}}$ , starting with the expression for  $\omega - \tilde{\mathcal{L}}$  in Eq. (B21), subtract the penultimate ( $M$ th) block row from the final [ $(M + 1)$ th] one. Then add the last block column from the penultimate block column. These two operations have the effect of eliminating the leftmost  $-\mathbb{1}$  block in the  $(M + 1)$ th block row and replacing  $R_{M-1}$  with  $R_{M-1} + R_M$  at the top of the  $M$ th block column. Iterate this process until obtaining the matrix in Eq. (B22).

To find the spectrum of  $S$ , we note that

$$S(p' | p) = M \delta_{\mu\mu'} \delta_{\nu\nu'} - \sum_{l=1}^M \langle \mu' | H_l | \mu \rangle \langle \nu | H_l | \nu' \rangle, \quad (\text{B25})$$

where each  $p_r = p(\mu_r, \nu_r) \in \{1, \dots, 8\}$  is a composite index, as described above. We find

$$\Gamma^\delta A_p \Gamma^\delta = \sum_{p'} \Delta_{p,p'}^\delta A_{p'} \quad (\text{B26})$$

with

$$\Delta^{1,2} = \Gamma^1 \oplus \pm\Gamma^1, \quad \Delta^{3,4} = \Gamma^{54} \oplus \mp\Gamma^{54}. \quad (\text{B27})$$

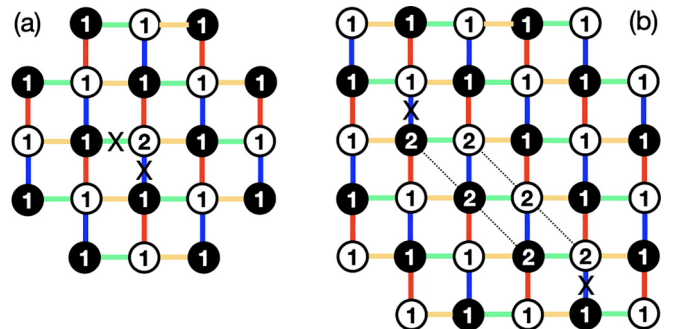


FIG. 20. Finite lifetime modes of the Liouvillian  $\mathcal{L}$ , with sites labeled by their  $q_r$  labels. (a) A configuration with  $s = 4$ , and (b) a string defect with  $s = 4$ . In both cases,  $\omega = -2/\gamma$  as  $\gamma \rightarrow \infty$  is the relaxation rate.

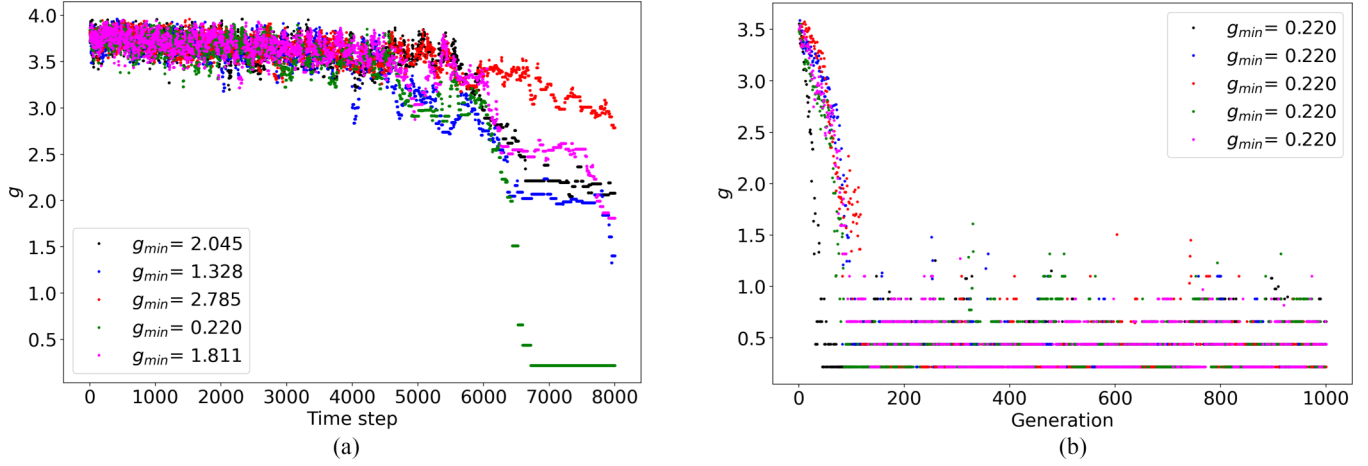


FIG. 21. Different runs of simulated annealing and the genetic algorithm for  $\gamma = 0.11$ ,  $N_x = N_y = 6$ , and all  $J_\delta = 1$  corresponding to an even sum of occupation numbers in Prosen’s generalized Bogoliubov transformation: (a) Simulated annealing (SA) versus the (b) genetic algorithm (GA). Each color depicts a run with a (a) randomly chosen initial configuration for SA, (b) randomly chosen initial population for GA. Parameters used: (a)  $\alpha = 10$ ,  $T_0 = 100$ , 20 time steps in a cycle. (b) Population size was 100. ( $g_{\min}$  refers to the minimum value of the gap encountered in that particular run.)

For example,

$$\begin{aligned}
 \Gamma^1 A_1 \Gamma^1 &= \Gamma^1 |1\rangle\langle 1| \Gamma^1 = +|3\rangle\langle 3| = +A_3 \\
 \Gamma^2 A_5 \Gamma^2 &= \Gamma^2 |1\rangle\langle 4| \Gamma^2 = -|3\rangle\langle 2| = +A_7 \\
 \Gamma^3 A_6 \Gamma^3 &= \Gamma^3 |2\rangle\langle 3| \Gamma^3 = -|1\rangle\langle 4| = -A_5 \\
 \Gamma^4 A_3 \Gamma^4 &= \Gamma^4 |3\rangle\langle 3| \Gamma^4 = +|4\rangle\langle 4| = -A_4.
 \end{aligned}
 \tag{B28}$$

Note that  $\Gamma^{54} = \mathbb{1} \otimes X$ . Since  $\Gamma^1$  and  $\Gamma^{54}$  commute, we may find a common basis:

$$\varphi_1 = \begin{pmatrix} 1 \\ 1 \\ 1 \\ 1 \end{pmatrix}, \quad \varphi_2 = \begin{pmatrix} 1 \\ -1 \\ 1 \\ -1 \end{pmatrix}, \quad \varphi_3 = \begin{pmatrix} 1 \\ 1 \\ -1 \\ -1 \end{pmatrix}, \quad \varphi_4 = \begin{pmatrix} 1 \\ -1 \\ -1 \\ 1 \end{pmatrix}.
 \tag{B29}$$

In this basis, we have

$$\begin{aligned}
 \tilde{\Delta}^1 &= \text{diag}(+, +, -, -, +, +, -, -) \\
 \tilde{\Delta}^2 &= \text{diag}(+, +, -, -, -, -, +, +) \\
 \tilde{\Delta}^3 &= \text{diag}(+, -, +, -, -, +, -, +) \\
 \tilde{\Delta}^4 &= \text{diag}(+, -, +, -, +, -, +, -).
 \end{aligned}
 \tag{B30}$$

The eigenvalues of  $\mathcal{S}$  are thus given by

$$s(q_1, \dots, q_N) = \sum_{\mathbf{R}} \sum_{\delta=1}^4 (1 - \tilde{\Delta}^\delta(q_{\mathbf{R}}) \tilde{\Delta}^\delta(q_{\mathbf{R}+\delta})), \tag{B31}$$

where each  $q_r \in \{1, \dots, 8\}$  and the values  $\tilde{\Delta}^\delta(q)$  are given in Eq. (B30). The  $q$  values label the linear combinations of

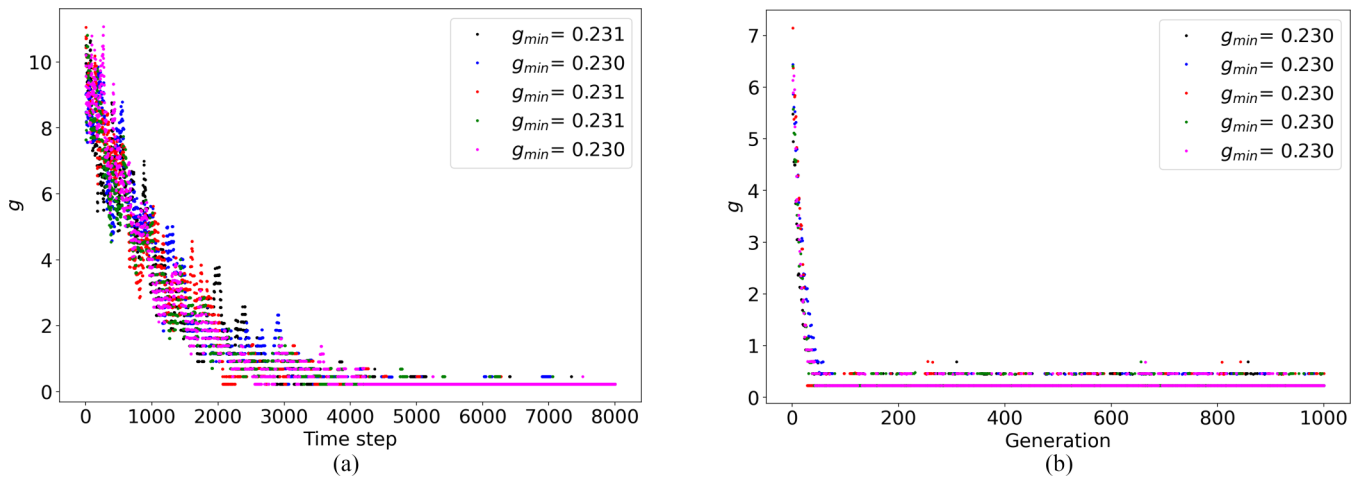


FIG. 22. Different runs of simulated annealing and the genetic algorithm for  $\gamma = 4.06$ ,  $N_x = N_y = 6$  and all  $J_\delta = 1$  corresponding to an even sum of occupation numbers in Prosen’s generalized Bogoliubov transformation: (a) Simulated annealing (SA) versus the (b) genetic algorithm (GA). Each color depicts a run with a (a) randomly chosen initial configuration for SA, (b) randomly chosen initial population for GA. Parameters used: (a)  $\alpha = 10$ ,  $T_0 = 100$ , 20 time steps in a cycle. (b) Population size was 100. ( $g_{\min}$  refers to the minimum value of the gap encountered in that particular run.)



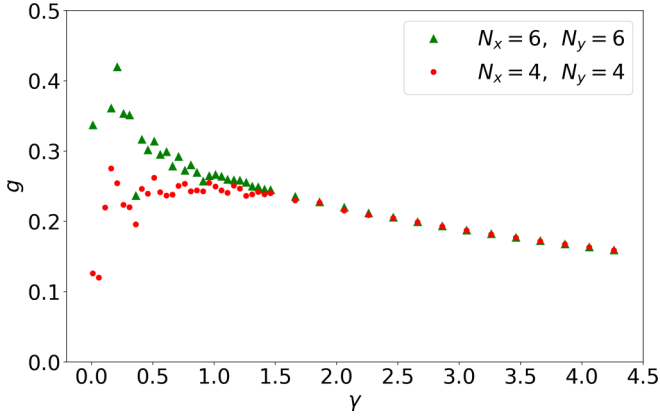


FIG. 23. Liouvillian gap,  $g$ , versus  $\gamma$  obtained over different runs of simulated annealing with  $(J_1, J_2, J_3, J_4) = (3, 4, 1, 2)$  for system sizes  $4 \times 4$  and  $6 \times 6$  and even  $f$  parity. We used  $\alpha = 10$ ,  $T_0 = 100$  and a cycle consisted of 20 time steps. The number of runs was 10 for  $4 \times 4$  and 5 for  $6 \times 6$ . Some data points that are present at greater values of  $g$  are not shown in this cropped plot to focus on the features near the cusps in the plot.

single-site density matrices associated with the eight common eigenvectors of the matrices  $\Delta^\delta$ , i.e.,  $\begin{pmatrix} \varphi_\eta \\ 0 \end{pmatrix}$  and  $\begin{pmatrix} 0 \\ \varphi_\eta \end{pmatrix}$ , with index  $\eta \in \{1, 2, 3, 4\}$ .

Clearly any configuration with all  $q_r$  equal will be a NESS, with  $\mathcal{S}$  eigenvalue  $s = 0$ . In Fig. 20 we sketch the configurations for two excited (i.e., decaying) modes, with nonzero eigenvalues of  $\mathcal{S}$ . Figure 20(a) depicts a configuration with a single site defect, an isolated  $q = 2$  state in a sea of  $q = 1$ . According to the rules derived here, Fig. 20(a) has “bad” bonds (labeled with an X) for which  $\tilde{\Delta}^\delta(q) \tilde{\Delta}^\delta(q') = -1$ , resulting in an eigenvalue  $s = 4$ . Figure 20(b) features

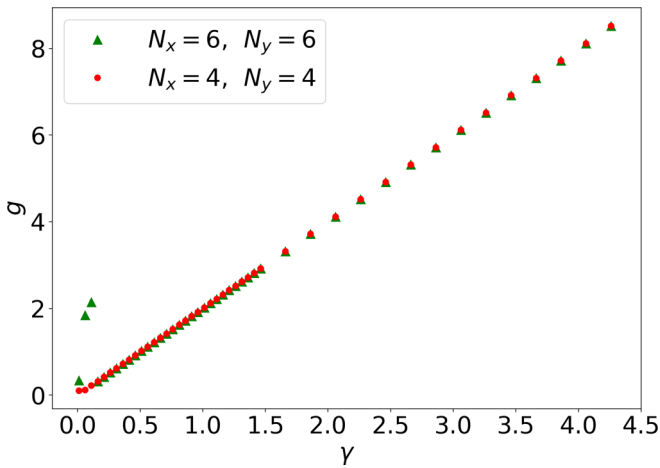


FIG. 24. Liouvillian gap,  $g$ , versus  $\gamma$  obtained over different runs of simulated annealing with  $(J_1, J_2, J_3, J_4) = (3, 4, 1, 2)$  for system sizes  $4 \times 4$  and  $6 \times 6$  and odd  $f$  parity. We used  $\alpha = 10$ ,  $T_0 = 100$  and a cycle consisted of 20 time steps. The number of runs was 10 for  $4 \times 4$  and 5 for  $6 \times 6$ .

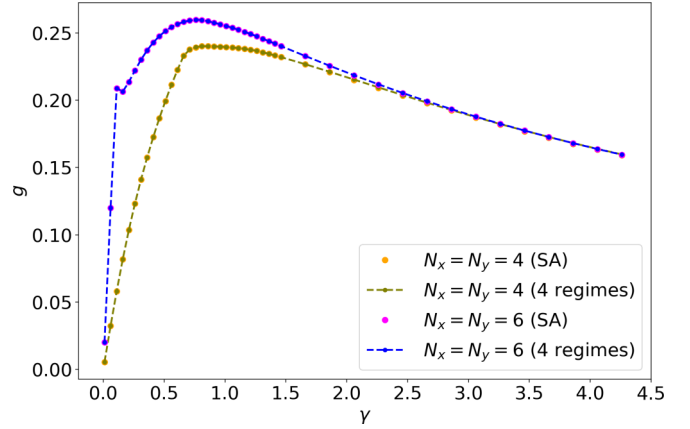


FIG. 25. SA and the phases are described in the text. Here  $(J_1, J_2, J_3, J_4) = (3, 4, 1, 2)$  and the  $f$  parity is even. The four regimes for  $4 \times 4$  are separated by  $\gamma_1^* = 0.71$ ,  $\gamma_2^* = 0.81$ , and  $\gamma_3^* = 1.26$ , and the four regimes for  $6 \times 6$  are separated by  $\gamma_1^* = 0.11$ ,  $\gamma_2^* = 1.06$ , and  $\gamma_3^* = 1.26$ .

two parallel diagonal line defects, there are also two bad bonds, but with a string connecting them, again giving  $s = 4$ . Both these configurations are highly degenerate. In the case of open boundary conditions, the string can run to a boundary, and one has a defect state with  $s = 2$ . Numerically, though, we find  $s = 2$  to be the lowest eigenvalue of  $\mathcal{S}$  even with periodic boundary conditions (Fig. 14).

In summary, we have analytical arguments for  $\omega \propto \gamma$  as  $\gamma \rightarrow 0$  and  $\omega \propto \gamma^{-1}$  as  $\gamma \rightarrow \infty$  based on perturbation theory, but the analytical value of the coefficient is twice that obtained from the numerical analysis. For  $\gamma \rightarrow 0$ , this might be because the actual first decay mode corresponds to a gauge field configuration that is not translationally invariant. In both limits, the discrepancy could also be because the vacuum state corresponding to the Bogoliubov particles is a linear combination of both even  $c$ -particle parity and odd  $c$ -particle parity states which complicates the implementation of the parity-related constraint.

### APPENDIX C: COMPUTATIONAL PROCEDURE

In our computations, we try to optimize the Liouvillian gap (corresponding to a given field configuration)  $g$  over the space of all possible field configurations,  $\mathcal{G} = \{u_R^\delta, u_r^\delta\}$ . We do this to obtain an estimate of the Liouvillian gap,  $g = \min_{\mathcal{G}} g_{\mathcal{G}}$ . Simulated annealing and the genetic algorithm are two commonly used optimization techniques.

In simulated annealing, we pick an initial configuration,  $\mathcal{G}$ , randomly and in each step, we change the sign of a randomly chosen gauge field. We then accept the change with the probability  $e^{-[g(t+1) - (g(t))]/T}$  where  $T$  is a temperature that we keep annealing as given by a cooling function, say once every 20 steps. After every cycle of 20 steps, we anneal the temperature as given by the following cooling function:  $T = T_0 / (1 + \alpha n_{\text{cyc}})$  where  $T_0$  is the initial temperature,  $\alpha$  is a parameter that we can control to set the cooling function and  $n_{\text{cyc}}$  is the cycle number [22]. We start with a different

initial configuration for each run and pick the minimum value of the gap obtained over different runs as our estimate of the Liouvillian gap. Increasing the number of steps and adjusting the cooling rate could help reduce the spread of data.

On the other hand, the genetic algorithm that we use to estimate the was as follows. For a given gauge field configuration  $\mathcal{G} = \{u_R^\delta, u_r^5\}$  we find the smallest relaxation rate gap  $g_F$  by solving for the spectrum of  $\mathcal{W}$  using Prosen's method [2]. In the genetic algorithm, the fitness function is given by the gap  $g_G$  and we try to further minimize this by varying over  $\mathcal{G}$ . We start with a population of randomly chosen individuals (field configurations). We find individuals with low values of gap perform crossovers and mutate by flipping the sign at some places. We then calculate the gaps for the individuals in the new population and repeat the same process.

We again do this over different runs, i.e., by starting with different randomly chosen initial populations. We pick the minimum  $g$  value obtained over different runs to be the estimate of the gap. Increasing the population size, letting the simulation run for a larger number of generations, etc. can be used to reduce the spread of data over different runs.

We see from a few trials that simulated annealing and the genetic algorithm give similar results for the even parity calculation. The runs for a few cases are shown in Fig. 21 and Fig. 22.

#### APPENDIX D: SOME FLUX CONFIGURATIONS FROM SIMULATED ANNEALING

Here we list some flux configurations for first decay modes obtained from simulated annealing. Relative to the NESS where all the gauge-invariant  $\mathbb{Z}_2$  data are set to  $-1$ , we list all the  $+1$  defects (i.e., plaquette fluxes and Wilson phases). As noted in the text, it may be that each of the states listed here may be describable as having fewer defects with respect to others among the exponentially many ( $2^{3N+1}$ ) states in the NESS block.

For  $N_x = N_y = 4, J_1 = J_2 = J_3 = J_4 = 1$ :

(1)  $\gamma < 0.36$ :  $\Phi_{2,2}^-, \Phi_{4,2}^+, \Phi_{1,3}^+, \Phi_{1,1}^-, \Phi_{2,4}^+, \Phi_{4,4}^+, \Omega_{1,3}^+, \Omega_{1,1}^-, \Psi_{2,4}^-, \Psi_{4,4}^+, W_y$

(2)  $0.36 \leq \gamma < 1.86$ :  $\Phi_{1,1}^+, \Phi_{2,2}^-, \Phi_{2,2}^+, \Phi_{3,3}^-, \Phi_{1,1}^-, \Phi_{2,4}^+, \Psi_{4,2}^-$

(3)  $\gamma \geq 1.86$ :  $\Phi_{1,1}^+, \Phi_{3,1}^+, \Phi_{1,3}^-, \Phi_{3,3}^-, \Phi_{3,3}^+, \Phi_{2,4}^+, \Phi_{3,1}^-, \Phi_{4,4}^+, \Psi_{2,2}^-$

For  $N_x = N_y = 6, J_1 = J_2 = J_3 = J_4 = 1$ :

(1)  $\gamma < 0.41$ :  $\Phi_{1,1}^+, \Phi_{4,2}^-, \Phi_{3,3}^-, \Phi_{5,3}^-, \Phi_{1,3}^+, \Phi_{4,4}^-, \Phi_{6,4}^-, \Phi_{1,5}^-, \Phi_{3,5}^-, \Phi_{4,4}^+, \Phi_{3,5}^-, \Phi_{4,6}^-, \Phi_{6,6}^-, \Phi_{1,1}^-, \Phi_{3,1}^+, \Phi_{6,6}^+, \Omega_{4,2}^+, \Omega_{4,4}^-, \Psi_{3,3}^+, \Psi_{5,3}^-, W_x$

(2)  $0.41 \leq \gamma < 1.66$ :  $\Phi_{1,1}^+, \Phi_{3,1}^+, \Phi_{6,2}^-, \Phi_{1,3}^+, \Phi_{2,4}^-, \Phi_{3,3}^+, \Phi_{6,4}^-, \Phi_{2,4}^+, \Phi_{3,5}^-, \Phi_{1,5}^+, \Phi_{3,5}^-, \Phi_{4,6}^-, \Phi_{1,1}^+, \Phi_{2,6}^-, \Phi_{5,1}^+, \Phi_{6,6}^+, \Omega_{6,2}^-, W_x$

(3)  $\gamma \geq 1.66$ :  $\Phi_{1,1}^+, \Phi_{2,2}^-, \Phi_{3,1}^+, \Phi_{5,1}^+, \Phi_{3,3}^-, \Phi_{2,4}^-, \Phi_{4,4}^-, \Phi_{6,4}^-, \Phi_{1,5}^+, \Phi_{2,6}^-, \Phi_{3,5}^+, \Phi_{6,6}^-, \Phi_{2,6}^+, \Phi_{3,1}^-, \Omega_{1,1}^+$

For  $N_x = N_y = 4, (J_1, J_2, J_3, J_4) = (3, 4, 1, 2)$ :

(1)  $\gamma < 0.71$ :  $\Phi_{3,1}^+, \Phi_{3,3}^-, \Phi_{4,2}^+, \Phi_{1,3}^-, \Phi_{4,4}^-, \Phi_{1,1}^-, \Psi_{3,1}^-, \Psi_{1,3}^-, W_x, W_y$

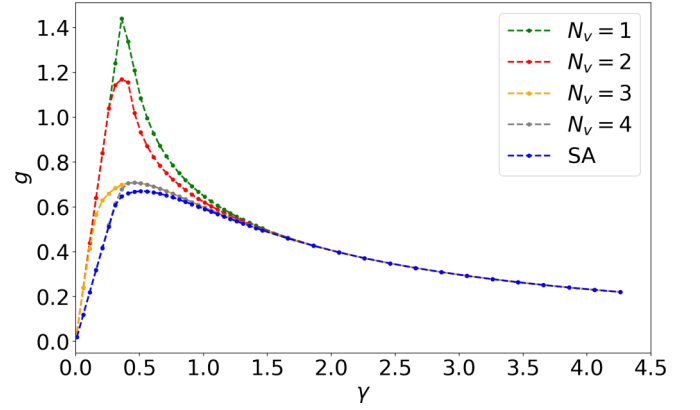


FIG. 26. The SA curve and the curves obtained by considering configurations with a given number of vortices  $N_v$ , as described in the text. Here all  $J_\delta = 1$  and the system size is  $4 \times 4$ .

(2)  $0.71 \leq \gamma < 0.81$ :  $\Phi_{1,1}^+, \Phi_{2,2}^-, \Phi_{3,1}^+, \Phi_{1,3}^-, \Phi_{2,2}^+, \Phi_{3,3}^-, \Phi_{4,4}^-, \Phi_{1,1}^+, \Phi_{2,4}^-, \Phi_{3,1}^-, \Psi_{1,3}^-, W_x$

(3)  $0.81 \leq \gamma < 1.26$ :  $\Phi_{3,1}^+, \Phi_{4,2}^-, \Phi_{2,2}^+, \Phi_{3,3}^-, \Phi_{1,3}^+, \Phi_{3,3}^+, \Phi_{4,4}^-, \Phi_{1,1}^+, \Phi_{3,1}^-, \Phi_{4,4}^+, \Psi_{1,3}^-, W_x$

(4)  $1.26 \leq \gamma$ :  $\Phi_{1,1}^+, \Phi_{2,2}^-, \Phi_{4,2}^+, \Phi_{2,2}^-, \Phi_{3,3}^-, \Phi_{4,2}^+, \Phi_{2,4}^-, \Phi_{3,3}^+, \Phi_{4,4}^-, \Phi_{1,1}^+, \Phi_{2,4}^+, \Phi_{3,1}^-, \Psi_{2,4}^-, W_x, W_y$

For  $N_x = N_y = 6, (J_1, J_2, J_3, J_4) = (3, 4, 1, 2)$ :

(1)  $\gamma < 0.11$ :  $\Phi_{2,2}^-, \Phi_{3,1}^+, \Phi_{4,2}^-, \Phi_{5,1}^+, \Phi_{6,2}^-, \Phi_{2,2}^+, \Phi_{3,3}^-, \Phi_{4,2}^+, \Phi_{5,3}^-, \Phi_{6,2}^+, \Phi_{1,3}^-, \Phi_{4,4}^+, \Phi_{5,3}^+, \Phi_{4,4}^-, \Phi_{5,5}^+, \Phi_{1,5}^+, \Phi_{3,5}^-, \Phi_{4,6}^-, \Phi_{2,6}^+, \Phi_{6,6}^+, \Omega_{3,3}^-, \Omega_{3,5}^+, \Psi_{2,4}^-, \Psi_{4,4}^-$

(2)  $0.11 \leq \gamma < 0.81$ :  $\Phi_{1,1}^+, \Phi_{2,2}^-, \Phi_{3,1}^+, \Phi_{2,2}^+, \Phi_{4,2}^+, \Phi_{1,3}^-, \Phi_{2,4}^-, \Phi_{4,4}^+, \Phi_{5,3}^-, \Phi_{6,4}^-, \Phi_{1,5}^-, \Phi_{2,4}^-, \Phi_{3,5}^+, \Phi_{4,4}^+, \Phi_{1,5}^+, \Phi_{2,6}^-, \Phi_{3,5}^+, \Phi_{5,5}^-, \Phi_{6,6}^-, \Phi_{1,1}^+, \Phi_{2,6}^+, \Phi_{4,6}^+, \Psi_{2,2}^-$

(3)  $0.81 \leq \gamma < 1.26$ :  $\Phi_{2,2}^-, \Phi_{3,1}^+, \Phi_{1,3}^-, \Phi_{2,2}^+, \Phi_{3,3}^-, \Phi_{4,2}^+, \Phi_{6,2}^+, \Phi_{3,3}^-, \Phi_{6,4}^-, \Phi_{3,5}^+, \Phi_{4,4}^-, \Phi_{5,5}^-, \Phi_{6,4}^+, \Phi_{1,5}^+, \Phi_{3,5}^-, \Phi_{3,1}^-, \Phi_{4,6}^+, \Phi_{6,6}^+, \Psi_{3,1}^-, W_x, W_y$

(4)  $1.26 \leq \gamma$ :  $\Phi_{1,1}^+, \Phi_{3,1}^+, \Phi_{4,2}^-, \Phi_{6,2}^-, \Phi_{2,2}^+, \Phi_{4,2}^+, \Phi_{5,3}^-, \Phi_{2,4}^-, \Phi_{5,3}^-, \Phi_{3,5}^+, \Phi_{2,6}^-, \Phi_{3,5}^+, \Phi_{5,5}^+, \Phi_{2,6}^+, \Phi_{4,6}^+, \Psi_{4,6}^-$

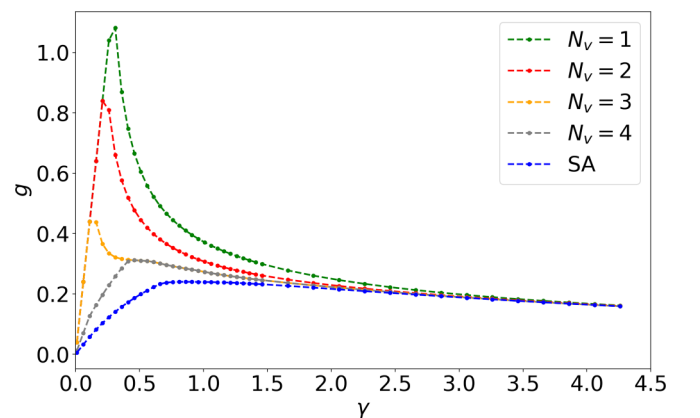


FIG. 27. The SA curve and the curves obtained by considering configurations with a given number of vortices  $N_v$ , as described in the text. Here  $(J_1, J_2, J_3, J_4) = (3, 4, 1, 2)$  and the system size is  $4 \times 4$ .

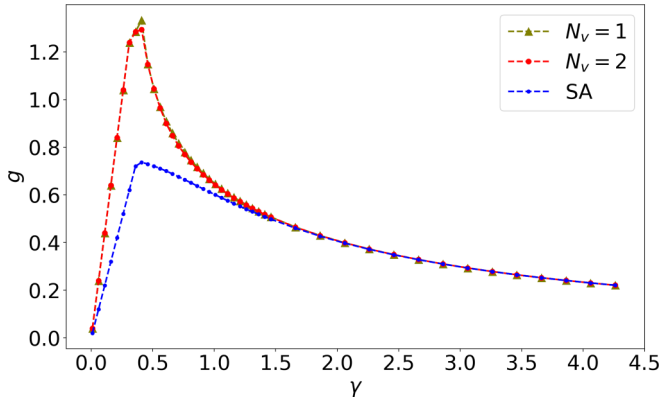


FIG. 28. The SA curve and the curves obtained by considering configurations with a given number of vortices  $N_v$ , as described in the text. Here all  $J_\delta = 1$  and the system size is  $6 \times 6$ .

#### APPENDIX E: OTHER COMPUTATIONAL RESULTS

This section contains results for larger system sizes for  $(J_1, J_2, J_3, J_4) = (3, 4, 1, 2)$  and an investigation of the spectrum by fixing the number of vortices. Figures 23–29 show the Liouvillian gap as a function of the dissipation strength  $\gamma$ . The smallest relaxation rates are shown in Figs. 23 and 24. Figure 25 is obtained from Fig. 23 in the same manner as Fig. 12 was obtained from Fig. 10, namely the gauge configurations with the lowest relaxation rates are collected and used as a pool to obtain an estimate of  $g(\gamma)$ . Figures 26–29 examine  $g(\gamma)$  for cases with a fixed number of plaquette vortices.

The  $N_v$ -limited data for the case with all  $J_\delta = 1$  and size  $4 \times 4$  is shown in Fig. 26. (See also Fig. 27 for the case when all the  $J_\delta$  are different.) Note that the  $N_v = 4$  results are in good agreement with the SA results. For the  $6 \times 6$

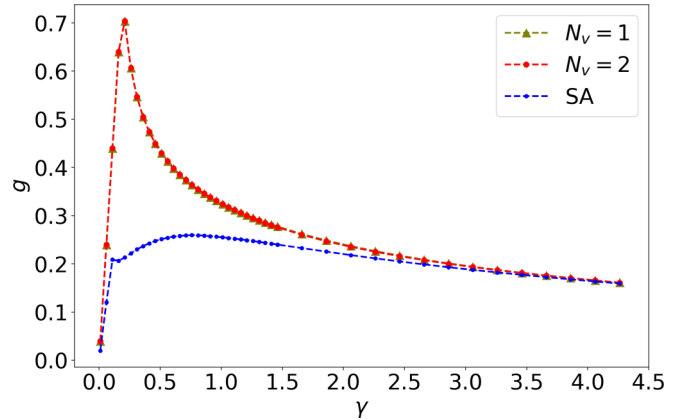


FIG. 29. The SA curve and the curves obtained by considering configurations with a given number of vortices  $N_v$ , as described in the text. Here all  $(J_1, J_2, J_3, J_4) = (3, 4, 1, 2)$  and the system size is  $6 \times 6$ .

case, the  $N_v = 1, 2$  results in Fig. 28 are quite far from the SA curve.

The behavior of the gap for the case  $(J_1, J_2, J_3, J_4) = (3, 4, 1, 2)$  for larger system sizes (obtained from SA) are shown in Figs. 23 and 24. SA and the phases are obtained as described before. While the shape of the curves is similar, we find two significant differences. First, from Fig. 25 it appears that SA has not found the lowest decay mode in the small  $\gamma$  regime, where the  $4 \times 4$  and  $6 \times 6$  SA results differ substantially. Second, as shown in Fig. 27, the  $N_v \leq 4$  sector does not yield a good approximation to the SA results, as it did for the case with all  $J_\delta = 1$ . We can also see from Fig. 29 that for the  $6 \times 6$  case with  $(J_1, J_2, J_3, J_4) = (1, 2, 3, 4)$ , the  $N_v \leq 2$  curves are quite far from the SA curve just as we saw in Fig. 28 for the case with all  $J_\delta = 1$ .

- [1] H.-P. Breuer and F. Petruccione, *The Theory of Open Quantum Systems* (Oxford University Press, Oxford, 2007).
- [2] T. Prosen, Third quantization: A general method to solve master equations for quadratic open fermi systems, *New J. Phys.* **10**, 043026 (2008).
- [3] N. Shibata and H. Katsura, Dissipative spin chain as a non-Hermitian Kitaev Ladder, *Phys. Rev. B* **99**, 174303 (2019).
- [4] D. Chruściński and S. Pascazio, A Brief history of the GKLS equation, *Open Syst. Inf. Dyn.* **24**, 1740001 (2017).
- [5] A. Kitaev, Anyons in an exactly solved model and beyond, *Ann. Phys.* **321**, 2 (2006).
- [6] E. H. Lieb, Two theorems on the Hubbard model, *Phys. Rev. Lett.* **62**, 1201 (1989).
- [7] H. Yao, S.-C. Zhang, and S. A. Kivelson, Algebraic spin liquid in an exactly solvable spin model, *Phys. Rev. Lett.* **102**, 217202 (2009).
- [8] C. Wu, D. Arovas, and H.-H. Hung,  $\Gamma$ -matrix generalization of the Kitaev model, *Phys. Rev. B* **79**, 134427 (2009).
- [9] We use the abbreviation NESS for both singular and plural “nonequilibrium steady state(s).”
- [10] X.-D. Dai, F. Song, and Z. Wang, Solvable BCS-Hubbard Liouvillians in arbitrary dimensions, *Phys. Rev. B* **108**, 115127 (2023).
- [11] H. Shackleton and M. S. Scheurer, companion paper, Exactly solvable dissipative spin liquid, *Phys. Rev. B* **109**, 085115 (2024).
- [12] V. V. Albert, Lindbladians with multiple steady states: theory and applications, [arXiv:1802.00010](https://arxiv.org/abs/1802.00010).
- [13] A. A. Dzhioev and D. S. Kosov, Nonequilibrium perturbation theory in Liouville–Fock space for inelastic electron transport, *J. Phys.: Condens. Matter* **24**, 225304 (2012).
- [14] V. Chua, H. Yao, and G. A. Fiete, Exact chiral spin liquid with stable spin Fermi surface on the kagome lattice, *Phys. Rev. B* **83**, 180412(R) (2011).
- [15] We find it convenient here to use expressions  $\Gamma^{\mu\nu} \equiv -\Gamma^{\nu\mu}$  with  $\mu > \nu$ .
- [16] There is of course a single remaining constraint associated with the condition  $\text{Tr} \rho = 1$ .
- [17] The regimes for size  $4 \times 4$  are separated at  $\gamma_1^* = 0.36$  and  $\gamma_2^* = 1.86$ , while those for size  $6 \times 6$  are separated at  $\gamma_1^* = 0.41$  and  $\gamma_2^* = 1.66$ . There could be degeneracies in the first

decay modes which could lead to there actually being a lesser number of regimes than what we obtained or the simulated annealing might not have discovered the actual first decay modes.

- [18] It is difficult for us to comment on the dependence of the gap on system size since the computations are quite intensive for system sizes larger than those shown here. However, from Fig. 12 it looks like the gap does not change much with system size. This is not so for the case where all the  $J_\delta$ 's are different as we shall see.
- [19] Modes with equal and opposite nonzero values of  $E_a$  correspond

to the same gap. We cannot rule out the possibility that there are degenerate lowest decay modes for the  $6 \times 6$  lattice with uniform  $J_\delta$  with  $\text{Re}E_a = 0$ .

- [20] T. Can, V. Oganesyan, D. Orgad, and S. Gopalakrishnan, Spectral gaps and midgap states in random quantum master equations, *Phys. Rev. Lett.* **123**, 234103 (2019).
- [21] R. A. Horn and C. R. Johnson, *Matrix Analysis* (Cambridge University Press, Cambridge, UK, 1985).
- [22] J. F. D. Martín and J. R. Sierra, A comparison of coolingschedules for simulated annealing, in *Encyclopedia of Artificial Intelligence* (IGI Global, 2009).